ปฏิกิริยารีฟอร์มมิ่งของมีเทนโดยใช้คาร์บอนไดออกไซด์บนตัวเร่งปฏิกิริยานิกเกิล
ชนิดที่มีตัวรองรับ

นางสาวนุชชนก ยุ้นพันธ์
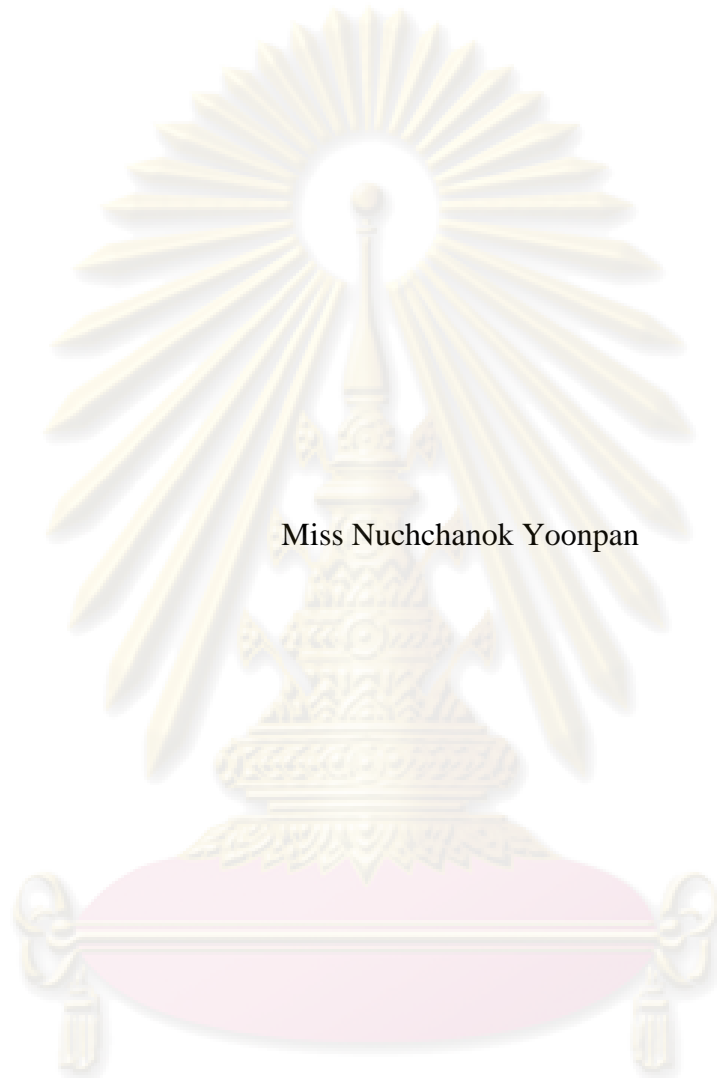
REFORMING REACTION OF METHANE BY CARBON DIOXIDE OVER SUPPORTED NICKEL CATALYSTS

Miss Nuchchanok Yoonpan

A Thesis Submitted in Partial Fulfillment of the Requirements

for the Degree of Master of Engineering Program in Chemical Engineering

Department of Chemical Engineering

Faculty of Engineering

Chulalongkorn University

Academic Year 2008

Thesis Title   REFORMING REACTION OF METHANE BY CARBON DIOXIDE OVER SUPPORTED NICKEL CATALYSTS

By   Miss Nuchchanok Yoonpan

Field of Study   Chemical Engineering

Advisor   Suphot Phatanasri, Ph.D

Accepted by the Faculty of Engineering, Chulalongkorn University in Partial Fulfillment of the Requirements for the Master's Degree

....Dean of the Faculty of Engineering

(Associate Professor Boonsom Lerdhirunwong, Dr.Ing.)

THESIS COMMITTEE

.....................................Chairman

(Assistant Professor Montree Wongsri, D.Sc.)

.... Advisor

(Suphot Phatanasri, Ph.D.)

.... Co-Advisor

(Professor Piyasan Praserthdam, Dr.Ing.)

.... Examiner

(Assistant Professor Bunjerd Jongsomjit, Ph.D.)

.... External Examiner

(Soipatta Soisuwan, D.Eng.)

นุชชนก ยุ้นพันธ์: ปฏิกิริยารีฟอร์มมิ่งของมีเทนโดยใช้คาร์บอนไดออกไซด์บนตัวเร่ง
ปฏิกิริยานิกเกิลชนิดที่มีตัวรองรับ (REFORMING REACTION OF METHANE BY
CARBON DIOXIDE OVER SUPPORTED NICKEL CATALYSTS) อ.ที่ปรึกษา
วิทยานิพนธ์หลัก: อ.ดร.สุพจน์ พัฒนะศรี, อ.ที่ปรึกษาวิทยานิพนธ์ร่วม: ศ.ดร.ปิยะสาร
ประเสริฐธรรม, 74 หน้า

ปฏิกิริยารีฟอร์มมิ่งของมีเทนด้วยคาร์บอนไดออกไซด์ถูกกระทำบนตัวเร่งปฏิกิริยานิกเกิล
บนตัวรองรับ ในงานวิจัยนี้ได้ศึกษาผลกระทบตัวรองรับตัวเร่งปฏิกิริยานิกเกิลที่มีต่อความว่องไวใน
การเกิดปฏิกิริยา ซึ่งจะทำการศึกษาตัวรองรับสองชนิดคืออะลูมินาที่มีความแตกต่างของเฟสและซี
โอไลท์ จากการทำการศึกษาพบว่า 7%Ni/50%χ-γ-alumina มีค่าร้อยละการเปลี่ยนแปลงของสารตั้ง
ต้นสูงกว่าตัวเร่งปฏิกิริยาตัวอื่นๆ รวมถึงมีค่าความต้านทานการเกิดโค้กที่สูงกว่าด้วย เมื่อ
เปรียบเทียบตัวรองรับตัวเร่งปฏิกิริยาอะลูมินาที่มีเฟสผสมกับตัวรองรับตัวเร่งปฏิกิริยาซีโอไลท์วาย
พบว่า ตัวเร่งปฏิกิริยาที่อยู่บนตัวรองรับอะลูมินาเฟสผสมให้ค่าร้อยละการเปลี่ยนแปลงของสารตั้ง
ต้นสูงกว่าตัวเร่งปฏิกิริยาบนตัวรองรับซีโอไลท์ อีกทั้งยังมีความเสถียรมากกว่าอีกด้วย นอกจากนั้น
งานวิจัยนี้ทำการเปรียบเทียบตัวเร่งปฏิกิริยานิกเกิลบนตัวรองรับซิลิกา-แมกนีเซียมออกไซด์ที่ใช้ใน
อุตสาหกรรมกับตัวเร่งปฏิกิริยานิกเกิลบนตัวรองรับอะลูมินาเฟสผสมที่เตรียมขึ้น พบว่า ตัวเร่ง
ปฏิกิริยานิกเกิลบนตัวรองรับซิลิกา-แมกนีเซียมออกไซด์ให้ค่าร้อยละการเปลี่ยนแปลงของสารตั้ง
ต้นสูงกว่าตัวเร่งปฏิกิริยานิกเกิลบนตัวรองรับอะลูมินาเฟสผสม แม้ว่าตัวเร่งปฏิกิริยานิกเกิลบนตัว
รองรับซิลิกา-แมกนีเซียมออกไซด์ให้ค่าร้อยละการเปลี่ยนแปลงของสารตั้งต้นสูงกว่าตัวเร่งปฏิกิริยา
นิกเกิลบนตัวรองรับอะลูมินาเฟสผสม แต่ตัวเร่งปฏิกิริยานิกเกิลบนตัวรองรับซิลิกา-แมกนีเซียม
ออกไซด์มีความเสถียรน้อยกว่านิกเกิลบนตัวรองรับอะลูมินาเฟสผสม

ภาควิชา.............วิศวกรรมเคมี........... ลายมือชื่อนิสิต...นุชชนก ยุ้นพันธ์...............

สาขาวิชา...........วิศวกรรมเคมี.......... ลายมือชื่อ อ.ที่ปรึกษาวิทยานิพนธ์หลัก.............

ปีการศึกษา..........2551.................... ลายมือชื่อ อ.ที่ปรึกษาวิทยานิพนธ์ร่วม..............

##50703271: MAJOR CHEMICAL ENGINEERING
KEYWORDS: CARBON DIOXIDE REFORMING/ ALUMINA-SUPPORTED NICKEL CATALYST/ PHASE ALUMINA

NUCHCHANOK YOONPAN: REFORMING REACTION OF METHANE BY CARBON DIOXIDE OVER SUPPORTED NICKEL CATALYSTS. ADVISOR: SUPHOT PHATANASRI, Ph.D., CO-ADVISOR: PROF. PIYASAN PRASERTDAM, Dr.Ing., 74 pp.

Carbon dioxide reforming of methane was carried out on supported nickel catalysts. The effect of different types of supports on the activity of nickel catalysts was investigated. Two types of supports, i.e. alumina in different phases and zeolite Y were adopted in this study. It has been found that 7%Ni/50%χ-γ-alumina exhibited the highest conversion as well as the highest coke resistance of all the catalysts studied. When compared between the mixed phase alumina and zeolite Y supported nickel catalysts, the former was found to possess both higher activity and stability than the letter. In addition, the comparison of mixed phase alumina supported catalyst with the commercial silica-magnesium oxide supported one was also made for carbon dioxide reforming of methane at the same conditions. Though the commercial silica-magnesium oxide supported nickel catalyst exerted higher conversion than did the mixed phase alumina supported one; however, the mixed phase alumina supported catalyst still showed essentially better stability.

ศูนย์วิทยทรัพยากร
จุฬาลงกรณ์มหาวิทยาลัย

Department:....Chemical Engineering... Student's Signature:..Nuchchanok yoonpan

Field of Study:...Chemical Engineering... Advisor's Signature:...Suphot Phtanasri

Academic Year:...2008.................. Co-Advisor's Signature:..........

ACKNOWLEDGEMENTS

CONTENTS

ศูนย์วิทยทรัพยากร
จุฬาลงกรณ์มหาวิทยาลัย

LIST OF TABLES

LIST OF FIGURES

CHAPTER I

INTRODUCTION

1.1 Rationale

Recently, Global warming caused by an increasing amount of greenhouse gases has made greenhouse effect becomes a serious problem of the world. Therefore, there has been an increasing interest in the catalytic transformation of carbon dioxide, one of major greenhouse gases, into more useful or valuable compounds. One of an alternative choice to reduce greenhouse gases is carbon dioxide reforming of methane reaction. Carbon dioxide reforming of methane reaction is to produce syngas ($CO+H_2$), which can be used as feedstock for methanol, dimethyl ether production and/or Fischer-Tropsch synthesis. Hydrogen production was used in ammonia synthesis fuel cell and hydrogenation reaction, [Guo et. al, 2007]. CO_2 reforming of methane is highly endothermic reaction (Eq.1.1). It's normally accompanied by secondary reaction of the reverse water gas shift (Eq.1.2).

$$CH_4 + CO_2 \ \leftrightarrow \ 2H_2 + 2CO \qquad \Delta H° = 247 \ \ kJ/mol \qquad \text{(Eq.1.1)}$$

$$CO_2 + H_2 \ \leftrightarrow \ H_2O + CO \qquad \Delta H° = 41.2 \ kJ/mol \qquad \text{(Eq.1.2)}$$

In addition, this process is high energy consumption due to endothermic reaction. Also, one serious problem is deactivation of catalyst by carbon formation (Eq.1.3, Eq.1.4), [Kang et. al, 2007]. Much attention has been paid to research aiming to improve and develop catalyst having increased coke resistance.

$$CH_4 \ \leftrightarrow \ C \ + \ 2H_2 \qquad \Delta H° = 79.4 \ \ kJ/mol \qquad \text{(Eq.1.3)}$$

$$2CO \ \leftrightarrow \ C \ + \ CO_2 \qquad \Delta H° = -172.2 \ \ kJ/mol \qquad \text{(Eq.1.4)}$$

Noble metal catalysts such as Pt, Rh, Ru suffer less coking but are substantially expensive which limits their use for industrial application. The supported nickel catalyst have been investigated for carbon dioxide reforming of methane

because they are quite economical compare to noble metal catalysts and possesses high activity as same as noble metal catalysts.

In addition to the metal, the catalyst support has also played an important role for carbon dioxide reforming of methane. Several research group studies have shown that nature of the support employed influences the catalytic activity. Amorphous solids (such as SiO_2 [Guo et. al, 2007], MgO [Wang et al., 2000], CeO_2 [Wang et al., 2000], α-Al_2O_3 [Wang et al., 1997]) and crystalline solids (such as zeolite [Pawelec et al., 2007], γ-alumina [Hao, 2008]) were examined as the catalyst support. Although many amorphous solid supports have been investigated and alumina exhibited the high initial activity but it is highly sensitive to coke formation [Kaengsilalai et. al, 2007]. Therefore, it is interesting to improve and develop nickel catalyst on alumina support for high activity and stability. Thus, this research has investigated the influences of phase of alumina (such as γ-Al_2O_3, χ-Al_2O_3, mixed phase between χ-and γ- of alumina) to catalytic activity of supported nickel catalysts in carbon dioxide reforming of methane.

1.2 Research objective

1. To study the effect of different kinds of supports (i.e. aluminosilicate and mixed phase of alumina) on catalytic activity, stability and coke formation in carbon dioxide reforming of methane.

2. To compare catalytic activity of nickel on mixed phase of alumina with nickel on silica-magnesium oxide commercial grade.

1.3 Research scopes

1. Prepare nickel loading approximately 7 wt % on mixed phase of alumina or aluminosilicate compounds. Catalysts were prepared by incipient wetness impregnation methods.

2. Characterize physical properties of supported nickel catalysts by using various techniques:

- X-ray diffractometry to determine crystallite size and phase.
- Nitrogen adsorption to determine BET specific surface area.
- Ammonia temperature program desorption to determine acidity of catalysts.
- Carbon monoxide chemisorption to determine quantities of active site of catalysts.
- Scanning Electron Microscopy (SEM-EDX) to study morphology and metal dispersion of catalysts.
- Transmission Electron Microscopy (TEM) to study size of nickel on supports.
- Thermogravimetric and differential thermal analysis (TG-DTA) to study carbon deposition.
- Hydrogen temperature program reduction to study reducing temperature.

3. Investigation of the performance of the prepared catalysts for carbon dioxide reforming of methane reaction under the following condition:

- Reaction temperature 700 °C.
- Atmospheric pressure.
- Reactant feed 50% methane in carbon dioxide.
- Space velocity 22,000 h^{-1}.
- The gas compositions of the reactants and products were analyzed by thermal conductivity detector-type gas chromatography.

This thesis is arranged as follows:

Chapter II explains basic information about supported nickel catalyst.

Chapter III presents the literature review of previous works related to this research.

Chapter IV describes synthesis methods for preparation of alumina in different phases and of nickel catalysts for carbon dioxide reforming of methane.

Chapter V presents experimental results and discussion.

Chapter VI presents overall conclusion of this research and recommendations for future research.
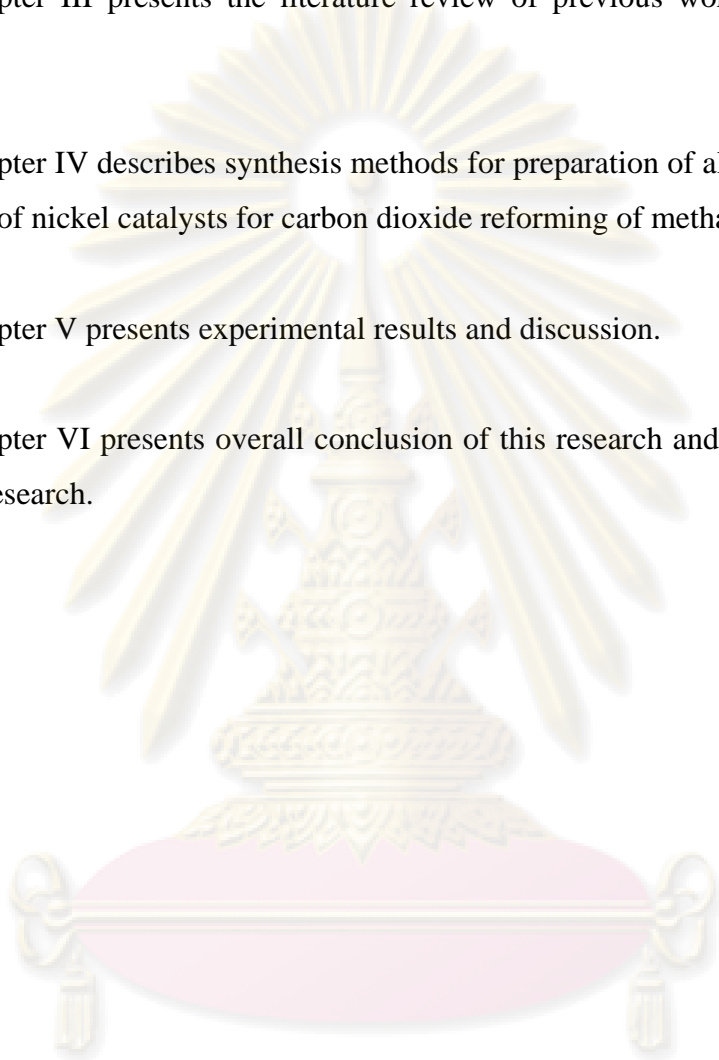
CHAPTER II

THEORY

2.1 Synthesis gas and hydrogen production

Synthesis gas is a mixture of carbon monoxide and hydrogen. It is currently produced by gasification of coal and combusted in gas turbines to get power. Another method to produce synthesis gas is methane reforming. In the reforming technology, there are three major processes for hydrogen and synthesis gas production from methane as follows.

- Steam reforming

  $CH_4 + H_2O \rightarrow CO + 3H_2$ $\Delta H°_{298} = 206.3$ kJ/mol (Eq.2.1)

- Carbon dioxide reforming

  $CH_4 + CO_2 \rightarrow 2CO + 2H_2$ $\Delta H°_{298} = 247.3$ kJ/mol (Eq.2.2)

- Partial oxidation

  $CH_4 + ½ O_2 \rightarrow CO + 2H_2$ $\Delta H°_{298} = -35.6$ kJ/mol (Eq.2.3)

  $CH_4 + 2O_2 \rightarrow CO_2 + 2H_2O$ $\Delta H°_{298} = -880$ kJ/mol (Eq.2.4)

The synthesis gas produced is converted to organic hydrocarbons by Fischer-Tropsch synthesis. Instead of supplying heat to the steam reforming process, a partial oxidation reaction is also carried out to make it self-sustaining. Another possible method to produce carbon monoxide and hydrogen from methane is the dry reforming of CO_2. The dry CO_2 reforming of methane is ≈20% more endothermic than steam reforming of methane (see Reactions Eq.2.1, 2.2) and partial oxidation in shows that Eq.2.3, 2.4. [Charoenseri, 2007]. Synthesis gas was also using feedstock for methanol synthesis. Another, hydrogen production was using feedstock for ammonia synthesis, hydrotreating, hydrogenation, and fuel cell power.

2.2 Reforming reaction of methane by carbon dioxide

2.2.1 Thermodynamics of carbon dioxide reforming of methane

The carbon dioxide reforming reaction has similar thermodynamic and equilibrium characteristics to steam reforming reaction. However, it generates syngas with lower H_2/CO ratio in Eq.2.5 and Eq.2.6.

$$CH_4 + CO_2 \rightarrow 2CO + 2H_2 \qquad \Delta H°_{298} = 247.3 \text{ kJ/mol} \qquad (Eq.2.5)$$
$$CH_4 + H_2O \rightarrow CO + 3H_2 \qquad \Delta H°_{298} = 206.3 \text{ kJ/mo} \qquad (Eq.2.6)$$
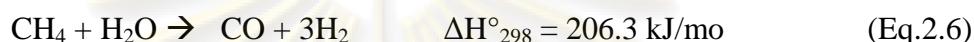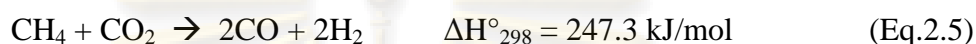
The carbon dioxide reforming of methane is conducted under conditions where carbon formation via catalytic cracking of methane (Eq.2.7) and/or Boudouard reaction (Eq.2.8) is thermodynamically feasible.

$$CH_4 \rightarrow C + 2H_2 \qquad \Delta H°_{298} = 74.9 \text{ kJ/mol} \qquad (Eq.2.7)$$
$$2CO \rightarrow C + CO_2 \qquad \Delta H°_{298} = -172.2 \text{ kJ/mol} \qquad (Eq.2.8)$$
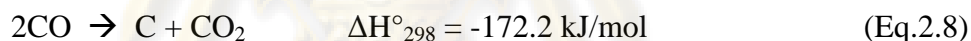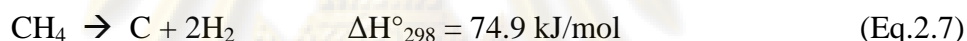
Other reactions which could also have an important influence on the overall product are:

$$CO_2 + H_2 \rightarrow CO + H_2O \qquad \Delta H°_{298} = 40 \text{ kJ/mol} \qquad (Eq.2.9)$$
$$C_{ads} + H_2O \rightarrow CO + H_2 \qquad \Delta H°_{298} = 131.4 \text{ kJ/mol} \qquad (Eq.2.10)$$
$$_{Cads} + CO_2 \rightarrow 2CO \qquad \Delta H°_{298} = 172.2 \text{ kJ/mol} \qquad (Eq.2.11)$$
$$_{Cads} + O_2 \rightarrow CO_2 \qquad \Delta H°_{298} = -393.7 \text{ kJ/mol} \qquad (Eq.2.12)$$
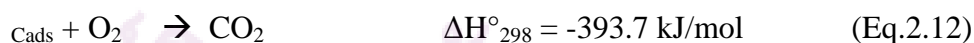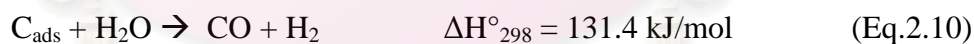
Theoretically, the carbon formed in reaction (Eq.2.7) should be rapidly consumed by the reverse of reaction (Eq.2.8), and by the steam/carbon gasification reaction Eq.2.10, Eq.2.11 and 2.12. [Kang et. al, 2007].

Practically, this reaction is almost always formed via the reverse water gas-shift (RWGS) reaction (Eq.2.9). Serious coke deposition on catalytic surface can be reduced by these two reactions. If the cracking reaction is faster than the carbon removal rate, there is formation of solid carbon, leading to catalyst deactivation and

plugging problem in the reactor. However, it should be noted that the formation of water is not desired in this reaction system because it decreases the selectivity of hydrogen.

2.2.2 Reaction mechanism of carbon dioxide reforming of methane

Many researches have been attempted to clarify the reaction mechanism in the carbon dioxide reforming of methane. The possible mechanism of this reaction over supported metal catalyst was proposed by Solymosi *et al.* (1991, 1993). The dissociation of methane with activation carbon formed at the end of reaction would produce activation of methane in shows that is Eq.2.13, 2.14, 2.15 and 2.16 as follows:

$$CH_4 \rightarrow CH_3^* + H^*, \quad (Eq.2.13)$$
$$CH_3^* \rightarrow CH_2^* + H^*, \quad (Eq.2.14)$$
$$CH_2^* \rightarrow CH^* + H^*, \quad (Eq.2.15)$$
$$CH^* \rightarrow C^* + H^*. \quad (Eq.2.16)$$

In general, there are many forms of deposited carbons, which are different in reactivity, i.e., adsorbed atomic carbon which is a highly reactive form, amorphous carbon, vermicular carbon, bulk nickel carbide, and crystalline graphitic carbon. The reactivity of deposited carbon depends on the type of catalytic surface, the temperature of its formation and the duration of thermal treatment. The dissociation of carbon dioxide with activation carbon formed at the end of reaction would produce activation of carbon monoxide in shows that is Eq.2.17. The formation of carbon from carbon monoxide with the precursor is shown by reaction (Eq.2.18).

$$CO_2 \rightarrow CO^* + O^*, \quad (Eq.2.17)$$
$$CO^* \rightarrow C^* + O^*. \quad (Eq.2.18)$$

Unless both methane and carbon dioxide can dissociate separately, their deposited products terminate the respective dissociation by covering the metal surfaces. The self-decomposition of both methane and carbon dioxide could be facilitated via reactions (Eq.2.19 to Eq.2.22). The dissociation of methane is enhanced by adsorbed

oxygen, while the dissociation of carbon dioxide is also promoted by adsorbed hydrogen and other methane residues. Therefore, the reactions of these surface species also need to be considered as the following reactions:

$$CO_2 + H^* \rightarrow \quad CO^* + OH^*, \quad \text{(Eq.2.19)}$$

$$CH_4 + O^* \rightarrow \quad CH_3^* + OH^*, \quad \text{(Eq.2.20)}$$

$$CH_x + O^* \rightarrow \quad CH_3^* + OH^*, \quad \text{(Eq.2.21)}$$

$$2OH \quad \rightarrow \quad H_2O^* + O^*. \quad \text{(Eq.2.22)}$$
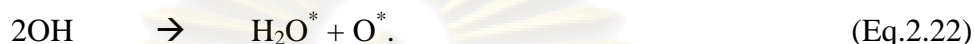
2.3 Supported catalyst

Zeolites (Greek, *zein*, "to boil"; *lithos*, "a stone") are water-aluminosilicates of natural or synthetic origin with highly structurees. They consist of SiO_4 and AlO_4^- tetrahedra, which are inerlinked through common oxygen atoms to give a three dimensional network through which long channels run.

In the interior of this channels, which are characteristic of zeolites, are water molecules and mobile alkali metal ions, which can be exchanged with other cations. These compensate for the excess negative charge in the anionic framework resulting from the aluminum content. The interior of the pore system, with its atomic-scale dimension, is the catalytically active surface of the zeolites. The inner pore structure depends on the composition, the zeolite type, and the cations. The general formular of zeolite is

$$M^I M^{II}_{0.5}[(AlO_2)_x \bullet (SiO2)_y \bullet (H_2O)_z]$$
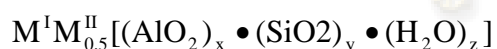
Where M^I and M^{II} are preferentially alkaline and alkaline earth metals. The indices x and y denote the oxide variables, and z is number the molecules of water of hydration. The composition is characterized by the Si/Al atomic ratio or by the molecular ratio M [Hagen, 2006].

$$M = \frac{SiO_2}{Al_2O_3}$$

2.3.1 Zeolite Y (Faujasite)

Faujasite was discovered in 1842 by Damour and is named for Barthélemy Faujas de Saint-Fond, a French geologist and volcanologist.

Structure

The faujasite framework consists of sodalite cages which are connected through hexagonal prisms. The pores are arranged perpendicular to each other. The pore, which is formed by a 12-membered ring, has a relatively large diameter of 7.4 Å. The inner cavity has a diameter of 12 Å and is surrounded by 10 sodalite cages. The unit cell is cubic with a length of 24.7 Å. Zeolite Y has a void fraction of 48 % and a Si/Al ratio of 2.43. It thermally decomposes at 793 °C.

Synthesis

Faujasite is synthesized as other zeolites from alumina sources such as sodium aluminate and silica sources such as sodium silicate. Other alumosilicates such as kaolin are used as well. The ingredients are dissolved in a basic environment such as sodium hydroxide aqueous solution and crystallized at 70 to 300 °C (usually at 100 °C). After crystallization the faujasite is in it is sodium form and must be ion exchanged with ammonium to improve stability. The ammonium ion is removed later by calcination which renders the zeolite in its acid form.

Use

Faujasite is used above all as a catalyst in fluid catalytic cracking to convert high-boiling fractions of petroleum crude to more valuable gasoline, diesel and other products. Zeolite Y has superseded zeolite X in this use because it is both more active and more stable at high temperatures due to the higher Si/Al ratio. It is also used in the hydrocracking units as a platinum/palladium support to increase aromatic content of reformulated refinery products. [Hagen, 2006].

2.3.2 Alumina

Aluminas are the most common commercial carriers because of their excellent thermal stability and wide range of chemical, physical, and catalytic properties. The alumina consists of more than a dozen well-characterized amorphous or crystalline structures. Which vary over wide range of surface area (0.5-600 m^2/g), pore size and pore distribution, and surface acidity.

Structure

The structure and properties of a given alumina depend on its preparation, purity, dehydration, and thermal treatment history. The more acidic, high-surface-area alumina hydrate produced at relatively low temperature by precipitation from either acidic or basic solutions and are transformed by dehydration and treatment at high temperature to 'transitional'β, γ, η, χ, δ, and θ- alumina and ultimately α-alumina, all of lower surface area and acidity. Some of the more well-known transformations are illustrated as a function of calcination temperature in Figure 3.1, and the physical and structural characteristics of important alumina phase formed at different calcinations temperatures are listed in Table 3.1.
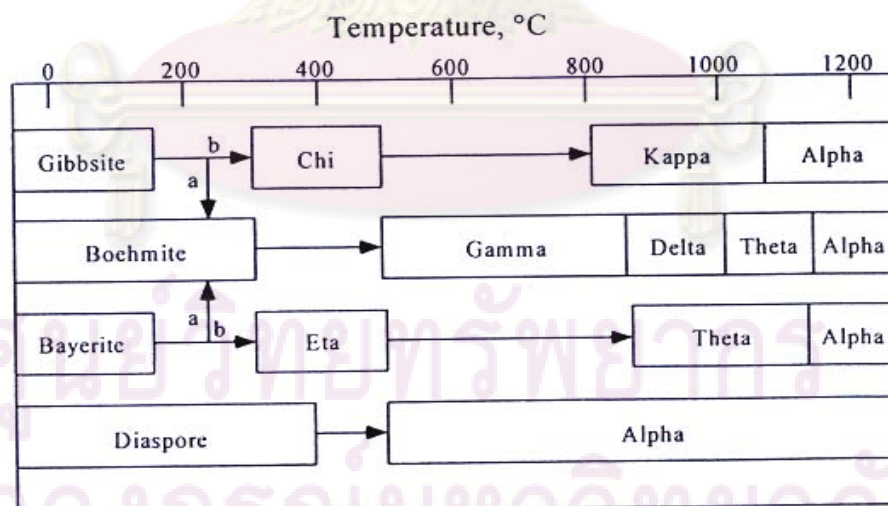
Figure 2.1 Alumina phase present at different temperatures: (a) corresponds to the path favored for fine crystals, (b) to the path for moist or particles.

Table 2.1 Physical and structural characteristic of common aluminum oxides.

T_{calc}(°C)	Alumina phase	SA, (m^2/g)	V_{pore}, (cm^3/g)	D_{pore}, (nm)
250	pseudoboehmite	390	0.50	5.2
450	γ- alumina	335	0.53	6.4
650		226	0.55	9.8
850		167	0.58	14
950	δ- alumina	120	0.50	16.6
1050	θ- alumina	50	0.50	28
1200	α- alumina	1-5		

Synthesis

The synthesis method for producing Al_2O_3 has many methods, which are under intensive worldwide investigated for powder preparation. The preparation of alumina by solvothermal method.

Solvothermal method has been developed from hydrothermal method for synthesis of metal oxide and binary metal oxide, by using solvent as the reaction medium under pressure and the temperature above its normal boiling point. The advantage of the solvothermal method are given products with uniform morphology, well controlled chemical position, narrow particle size distribution, controlled crystal structure, and controlled graines and morphologies can be controlled by process conditions such as solute concentration, reaction temperature, reaction time and type of solvent. The preparation method is described in the experimental section, chapter IV.

Use

It is used, for example, as a carrier in alkene and benzene hydrogenation, catalytic reforming, hydrotreating, emission control, methanol synthesis, the water gas shift reaction, and oxychlorination. Because its moderate acidity, it also finds application as a catalyst in a number of reactions required acid sites, e.g. the alkylation of phenol, the dehydration of formic acid, catalytic reforming, catalytic cracking and hydrogenation.

2.4 Metal catalyst

Group VIII metals (i.e. Pt, Pd, Rh, Ru) are reported to be effective catalysts in this reaction and less sensivity to coke formation. However, when one considers the high cost. Due to its availability and low cost, nickel is the most appropriate catalyst for the reaction. However, the Ni-based catalysts are readily deactivated by the deposition of carbon on the active centers. This situation leads to the need of developing Ni catalysts with improved activity and selectivity in order to prevent or reduce the formation of carbon.
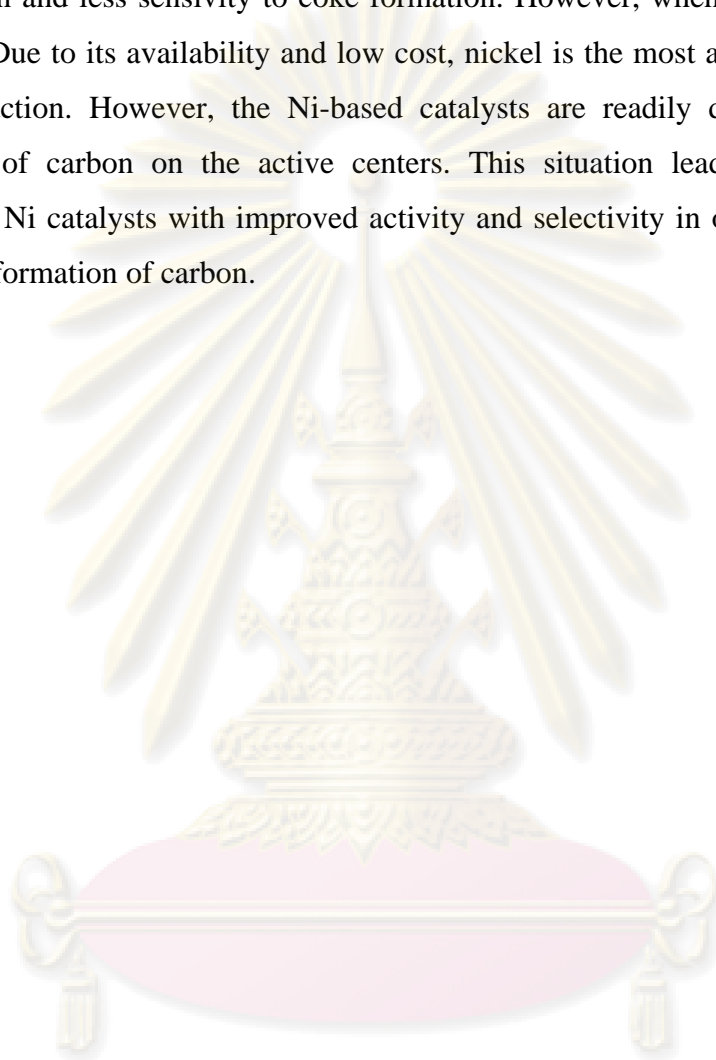
CHAPTER III

LITERATURE REVIEWS

This chapter presents the literature reviews for reforming of methane by carbon dioxide.

Effect of supported catalysts in reforming of methane by carbon dioxide

There are several studies of effect of supported catalyst in above reaction. Many researchers have been found better knowledge about effect of support on performance of catalyst. These reports are very useful and will use to develop works for the future.

In 1997, Shaobin Wang and G.Q.M. Lu (1997) studied effect of support phase on catalytic activity and carbon deposition were systematically investigated over nickel catalysts supported on Al_2O_3, SiO_2 and MgO for the reforming reaction of methane with carbon dioxide. It is found that both Ni/ γ -Al_2O_3 and Ni/ α -Al_2O_3 catalysts had very high CH_4 and CO_2 conversions. Conversions on the Ni/γ-Al_2O_3 catalyst were slightly higher than those on the Ni/α-Al_2O_3 catalyst at the same temperature. They proposed that this difference could be attributed to the stable allotropic form of α -alumina and its lower surface area. The low porosity decreased the amount of contact that the gas had with the catalyst surface and thus a lower conversion resulted. Comparing the amount of carbon deposition it is known that the coking on Ni/ α -Al_2O_3 higher than Ni/ γ -Al_2O_3 catalyst.They was concluded that the pore structure of the support and metal-support interaction signicantly affected the catalytic activity and coking resistance. Catalyst with well-developed porosity exhibited higher catalytic activity. Strong interaction between metal and the support made the catalyst more resistant to sintering and coking, thus resulting in a longer time of catalyst stability.

H.Y. Wang and E. Ruckenstein (2000) investigated the carbon dioxide reforming of methane over the reduced supported Rh (0.5 wt.%) catalysts. Two kinds of oxides, reducible (CeO_2, Nb_2O_5, Ta_2O_5, TiO_2, and ZrO_2) and irreducible (γ-Al_2O_3, La_2O_3, MgO, SiO_2, and Y_2O_3) were used as supports. They are found that the CO_2 conversion was always higher than that of CH_4, and the CO yield was always higher than that of H_2. A H_2/CO ratio below 1.0 was always obtained. The performance of the supported catalyst is strongly affected by the support. With the exception of Ta_2O_5, the reducible oxides provided much lower conversions of CH_4 and CO_2 and yields to CO and H_2 than the irreducible ones. For the irreducible oxides, the conversions and yields obtained after 0.5 hour on stream decreased in the sequence: $SiO_2 \approx MgO \approx \gamma$-$Al_2O_3 > Y_2O_3 > La_2O_3$; however, after 50 hour on stream the sequence became γ-$Al2O_3 \approx MgO > Y_2O_3 > SiO_2 \approx La_2O_3$. For the reducible oxides, the conversions and yields obtained after 0.5 hour on stream decreased in the sequence $Ta_2O_5 \approx TiO_2 \approx ZrO_2 > Nb_2O_5 > CeO_2$, while after 50 hour on stream in the sequence $ZrO_2 > Ta_2O_5 > CeO_2 \approx TiO_2 \approx Nb_2O_5$.

S. Murata et al. (2003) studied catalytic performance of nickel-loaded, zeolite-based support for CO_2 reforming of methane was investigated. Among the three zeolites employed (H-Y, H-mordenite, and Na-mordenite), H-mordenite was found to be the best support for the above reaction, probably due to its thermal stability. Comparing the activity of Ni/H-mordenite (Ni/HM) with conventional Ni/alumina catalyst (Ni/Al_2O_3) while while deactivation of the former proceeded at a slightly faster rate than that of the latter. It was also found that a physical mixture of alumina and zeolite, and composite support consisting of alumina and zeolite, became a more effective support than zeolite itself. The resulting Ni/H-mordenite-alumina catalyst (Ni/Mix or Ni/Cmp) showed the highest performance among the catalysts employed in the present study.

D. Halliche et al. (2005) investigated catalysts based on HZSM-5 (Si/Al = 14) and USY (Si/Al = 3.5) zeolites exchanged by a solution of nickel nitrate which Ni based on zeolites comparing Ni on alumina by impregnation method. They found Ni on alumina catalyst have a highest activity. The catalytic properties of the NiUSY and Ni/γ-Al_2O_3 catalyst have been found to be superior to those of NiZSM-5.

M. Nagai et al. (2006) studied CO_2 reforming of methane on the Rh/Al_2O_3 catalyst was performed using a flow microreactor at 773–973 K and studied effects of the catalyst pretreatment. They found that the oxidized/reduced Rh/Al_2O_3 catalyst had a higher activity than the oxidized catalyst. The Rh/CeO_2 catalyst is less active than the Rh/Al_2O_3 catalyst for the CO_2 reforming of methane, which the areal activity of the Rh/CeO_2 was close to Rh/Al_2O_3. Rh/CeO_2 catalyst occurred carbon deposition lower the Rh/Al_2O_3 catalyst.

Wang Rui et al. (2007) studied effect of metal-support interaction on coking resistant of Rh/Al_2O_3, Rh/SiO_2, and Rh/CeO_2 catalyst during CH_4/CO_2 reforming. It is found that the initial CH_4 activity decreased in the sequence $Rh/Al_2O_3 > Rh/SiO_2 > Rh/CeO_2$. Meanwhile, this result is also accordant with the sequence of Rh dispersion of catalysts. This implied that the sequence of exposed Rh surface area of reduced catalyst indeed coincides with the activity. In addition, the stability of catalyst after 25 hour of reaction increased in the order $Rh/SiO_2 < Rh/Al_2O_3 < Rh/CeO_2$ which is in the reverse order of the amount of deposition carbon. This suggests that the stability may be associated with the coking resistant of catalyst during CH_4/CO_2 reforming.

A. Kaengsilalai et al. (2007) investigated catalytic activity of Ni on a series of catalysts supported on the synthesized KH zeolite for the CO_2 reforming of methane. Eight percent Ni was impregnated onto the synthesized KH zeolites, which have different morphologies: called dog-bone, flower, and disordered shapes. The results showed that Ni supported on synthesized KH zeolites give very high activity on both CH_4 and CO_2 conversions of ≈85–95% and ≈85–90%, respectively. The CH_4 conversion of Ni supported on the disordered KH zeolite seemed to be lower than those of Ni supported on the other two KH zeolites. In other words, Ni/flower-shaped KH and Ni/dogbone-shaped KH did not give much different activity to convert both CH_4 and CO_2 to CO and H_2. This might result from the fact that the flower-shaped morphology was destroyed by the grinding force during catalyst preparation, and each petal of the flower became isolatable, presented as a dog-bone. Therefore, almost no difference in catalytic activity was observed. Thermogravimetric analysis (TGA) was employed to estimate the amount of carbon deposition. The result show that the

carbon deposition on spent Ni supported on flower-shaped and dog-bone-shaped KH zeolites was lower than that on the spent Ni supported on disordered KH zeolite.

Adolfo E. et al. (2008) studied influence of K, Sn, Mn and Ca on the behavior of a Ni-Al$_2$O$_3$ catalyst, prepared by a sol–gel method. A Ni-Al$_2$O$_3$ catalyst obtained via a sol–gel method showed an excellent performance in the reaction of methane dry reforming, with high and stable catalytic activity. The effect of the introduction of a 0.5 wt.% of the metals K, Ca, Sn and Mn, compared with the original catalyst, was studied. In the case of the Ca, Mn and Sn-modified catalysts, a dramatic reduction of catalytic activity and a significant increase in carbon deposition were observed during the period of time under study. The K modified catalyst showed low carbon and high stability of its catalytic activity. Compared with the unmodified catalyst, it showed a slight activity decrease of less than 4% in methane conversion. It has been proposed that potassium migrates from the support to the surface of nickel and neutralizes a fraction of the most active sites for the reforming reaction producing, as a consequence, a decrease in methane conversion.

CHAPTER IV

EXPERIMENTAL

In this chapter, the experimental section is divided into three sections. The first part involves the preparation of nickel catalyst on supported nickel catalysts in section 4.1. Secondly, the characterization of nickel catalyst on supported by using X-Ray Diffraction (XRD), Scanning Electron Microscopy (SEM-EDX), Nitrogen physisorption, CO chemisorption, Transmission Electron Microscopy (TEM), Ammonia Temperature Program Desorption (NH_3-TPD), Hydrogen Temperature Program Reduction (H_2-TPR), and Thermo gravimetric and differential thermal analysis (TG-DTA) are presented in section 4.2. Finally, the effects of preparation method of nickel catalyst on alumina and/or crystalline aluminosilicate in the carbon dioxide reforming of methane reaction are investigated in section 4.3.

In this study, HY-zeolite support was obtained from TOSOH Corporation which is the commercial grade. Alumina oxide was synthesized by solvothermal method. Using aluminum isopropoxide as source of alumina oxide. The catalysts of mixed phase of alumina obtained were also compared with nickel on silica-magnesium oxide commercial grade.

4.1. Catalyst preparation

4.1.1 Preparation of the Zeolite Y support

Zeolite Y (BET area 750 m^2/g), was obtained from TOSOH Corporation (Japan) in proton form with Si/Al = 7, 200. Before used, zeolite Y was dried at 110 °C and was subsequently calcined in stagnant air at 500 °C for 2 h.

4.1.2 Preparation of various phases of alumina supports by solvothermal

The details of chemicals for preparation of various phases Al_2O_3 supports are as follows:

1. Alumina Isopropoxide: AIP, $([(CH_3)_2CHO]_3Al)$ from Aldrich.
2. 1-Butanol, (C_4H_9OH) from Fluka.
3. Toluene, $(C_6H_5CH_3)$ from Fisher Scientific.
4. Methanol, (CH_3OH) from Merck.
5. Nitrogen, (N_2) from TIG.

15 grams of aluminum isopropoxide was suspended in 100 ml of desired organic solvent in a test tube, the organic solvents using in this experiments were toluene, 1-butanol and the mixed solvents thereof with desired composition, and then the test tube was placed in a 300 ml autoclave. An additional 30 ml of same solvent was placed in the gab between the autoclave wall and the test tube. The autoclave was completely purged with nitrogen, heated to a desired temperature at a rate of 2.5 $^\circ$C min $^{-1}$ and kept at that temperature for 2 h. After the autoclave was cooled to room temperature, the resulting product was repeatedly washed with methanol by vigorous mixing and centrifuging and then dried in air. The as-synthesized powders were calcined in air at 600 $^\circ$C for 6 h with a heating rate of 10°C/min. [J.Khom-in, 2007].

Table 4.1 χ/γ ratio in preparing catalysts of solvothermal method.

χ/γ ratio	In test tub, (ml)		In the gap between the autoclave wall and the test tube, (ml)	
	Toluene	1-Butanol	Toluene	1-Butanol
0/100	0	100	0	30
50/50	50	50	15	15
100/0	100	0	30	0

4.1.3 Nickel loading on supports

Ni-based catalysts was prepared with 7 wt% Ni and the catalysts were prepared by incipient wetness impregnation method using Ni $(NO_3)_2 \cdot 6H_2O$ (Merck) as the metal precursors. After loading nickel on the support, the catalyst samples were dried overnight at 110 $^{\circ}$C and were subsequently calcined in air at 500 $^{\circ}$C for 5 h which the incipient wetness impregnation procedure was as following:

1. Nickel nitrate (7%wt) was dissolved in deionized water in an equal volume to pore volume of catalyst.

2. The catalyst support was impregnated with aqueous solution of nickel by the incipient wetness technique. The solution was dropped slowly to the catalyst support.

3. The impregnated support was left to stand at room temperature for 4 hours to assure adequate distribution of metal complex. After that the catalyst was dried in the oven at 110 $^{\circ}$C overnight.

4. The catalyst was calcined in air at 500°C for 5 hours.

4.2. Catalyst characterization

4.2.1 X-ray diffraction pattern

The crystallinity of the prepared catalysts was identified using powder X-ray diffraction (XRD) by an X-ray diffractometer SIEMENS D 5000 connected with a personal computer with Diffract AT version 3.3 program for fully control of the XRD analyzer. The experiments were carried out by using Ni-filtered Cu K_α radiations with a generator voltage and current of 30 kV and 30 mA, respectively. A scan step of 0.04° was applied during a continuous run in the 6 –80° range.

4.2.2 Nitrogen physorption

The catalyst 0.2 gram was study BET surface area, pore volume and pore diameter were measured by N_2 adsorption–desorption isotherm at liquid nitrogen temperature (-196 ◦C) using a Micromeritics ASAP 2020. The surface area and pore distribution were calculated according to Brunauer-Emmett-Teller (BET) and Barret-Joyner-Halenda (BJH) methods, consecutively.

4.2.3 Temperature Programmed Desorption of Ammonia (NH₃-TPD)

The acid properties of prepared catalysts were observed by Temperature Programmed Adsorption of Ammonia (NH₃-TPD) equipment by using Micromeritics chemisorp 2750 Pulse Chemisorption System. In an experiment, about 0.10 g of the catalyst sample was placed in a quartz tube and pretreated at 200 °C in a flow of helium. The sample was saturated with 15%NH₃/He. After saturation, the physisorbed ammonia was desorped in a helium gas flow about 1.0 h. Then the sample was heated from 40 to 800 °C at a heating rate 10 °C /min. The amount of ammonia in effluent was measured via TCD signal as a function of temperature.

4.2.4 Scanning Electron Microscopy (SEM)

Scanning Electron Microscopy was employed for including the shape and size of the prepared zeolite crystal. The JEOL JSM-35 CF model at the Scientific and Technology Research Equipment Centre, Chulalongkorn University (STREC) was used for this purpose.

4.2.5 Transmission Electron Microscope (TEM)

The particle size and distribution of catalyst samples will be observed using JEOL-JEM 200CX transmission electron microscope operated at 100 kV.

4.2.6 CO Chemisorption

Static CO chemisorption at room temperature on the reduce catalysts will be used to determine the number of reduce surface nickel metal atoms. The total CO chemisorption will be calculated from the number of injection of a known volume. CO chemisorption will be carried out following the procedure using a Micrometritics Pulse Chemisorb 2750 instrument at the Analysis Center of Department of Chemical Engineering, Faculty of Engineering, Chulalongkorn University. In an experiment, about 0.20 g of the catalyst sample was placed in a quartz tube. Prior to chemisorption, the catalysts will be reduced at 600 ^{o}C for 1 hour after ramping up at a rate of 10 ^{o}C/min. After, carbon monoxide 86 microlite was inject to catalyst and repeat until desorption peak constant. Amount of carbon monoxide adsorption on catalyst was relative amount of active site.

4.2.7 Thermogravimetric and differential thermal analysis (TG-DTA)

The as-spun alumina fibers was subjected to the thermogravimetric and differential thermal analysis (Diamond Thermogravimetric and Differential Analyzer, TA Instruments SDT Q600) to determine the carbon content in the sample, as well as their thermal behaviors in the range of 10-800 ^{o}C. The analysis was performed at a heating rate of 10 ^{o}C /min in 100 ml/min flow of air.

4.2.8 Hydrogen Temperature Programmed Reduction (H$_2$-TPR)

The reducing temperatures of prepared catalysts were observed by Temperature Programmed Reduction of Hydrogen (H$_2$-TPR) equipment by using Micromeritics chemisorp 2750 Pulse Chemisorption System. In an experiment, about 0.20 g of the catalyst sample was placed in a quartz tube and pretreated at 200 $^{\circ}$C in a flow of nitrogen. The sample was reduced with 10%H$_2$/Ar. Then the sample was heated from 40 to 800 $^{\circ}$C at a heating rate 10 $^{\circ}$C /min. The amount of hydrogen consumption in effluent was measured via TCD signal as a function of temperature.

4.3. Reaction Testing

4.3.1 Chemical and Reagents

UHP Nitrogen Gas, 99.999% for pretreated catalyst.

UHP Hydrogen Gas, 99.999% for reduced catalyst.

Feed Gas: 50% Methane in Carbon dioxide for methane conversion.

4.3.2 Instrument and Apparatus

(a) Reactor: The reactor was a fixed bed reactor made from a stanlessstil tube with an inner diameter of 5.6 mm.

(b) Automatic Temperature and Controller: This unit consists of a magnetic switch connected to a variable voltage transformer and a temperature controller connected to a thermocouple attached to the catalyst bed in reactor. A dial setting established a set point at any temperature within the rage between 0°C to 1000°C.

(c) Electric Furnace: This supply the required heated to the reactor for reaction. The reactor could be operating at 700°C.

(d) Gas Controlling Systems: Gas was equipped with pressure regulator (0-120 psig), an on-off valve and needle valve were used to adjust flow rate of gas.

(e) Gas Chromatographs: Operating conditions were shown in Table 4.3.

Table 4.2 Operating condition gas chromatograph for CH_4/CO_2 to syngas.

Gas Chromatograph	Shimazu, GC 8A	Shimazu, GC 8A
Detector	TCD	TCD
Column	Porapack-Q	Molecular sieve 5A
Carrier gas	Argon	Argon
Carrier gas flow	30 ml/min	30 ml/min
Column Temperature		
- Initial	60 °C	60 °C
- Final	60 °C	60 °C
Detector temperature	100 °C	100 °C
Injector Temperature	100 °C	100 °C
Analyzed gas	CO_2	CH_4, CO, H_2

4.3.3 Reaction Method

The experiments were performed in a fixed-bed reactor, with an inner diameter of 5.6 mm, imbedded in an insulated electric furnace equipped with a temperature programmable controller. A K-type thermocouple was inserted into the catalyst bed to measure and control the bed temperature. The reactant gas stream consisted of CO_2 and CH_4 with a molar ratio of 1:1 at a total flow rate of 100 ml/min. A fresh 0.2 g catalyst sample was packed into the reactor and reduced in flowing hydrogen at 600 °C for 1 h and then was purged with flowing nitrogen at the reaction temperature for 45 min. The catalytic activity was studied at 700 °C. Figure 4.1 shown scheme diagram of reforming reaction of methane by CO_2. The gas compositions of the reactants and products were analyzed by Thermal Conductivity Detector-type gas chromatographs, Shimudzu GC-8A equipped with a Porapak-Q and Molecular sieve 5A packed column. The conversions of CH_4 and CO_2 and selectivity of H_2 and CO are defined in equation shows is Eq.4.1, 4.2, 4.3 and 4.4 as follows:

$$X_{CH_4} = \frac{[CH_4]_{in} - [CH_4]_{out}}{[CH_4]_{in}} \times 100 \qquad \text{(Eq.4.1)}$$

$$X_{CO_2} = \frac{[CO_2]_{in} - [CO_2]_{out}}{[CO_2]_{in}} \times 100 \qquad \text{(Eq.4.2)}$$

$$S_{H_2} = \frac{1}{2} \frac{[H_2]_{out}}{[CH_4]_{in} - [CH_4]_{out}} \times 100 \qquad \text{(Eq.4.3)}$$

$$S_{CO} = \frac{[CO]_{out}}{[CH_4]_{in} - [CH_4]_{out} + [CO_2]_{in} - [CO_2]_{out}} \times 100 \qquad \text{(Eq.4.4)}$$

Where $[CH_4]_{in}$ and $[CO_2]_{in}$ are the flow rates of the introduced reactants and $[CH_4]_{out}$, $[CO_2]_{out}$, $[H_2]_{out}$, and $[CO]_{out}$ are the flow rates of the corresponding compositions in the effluents.
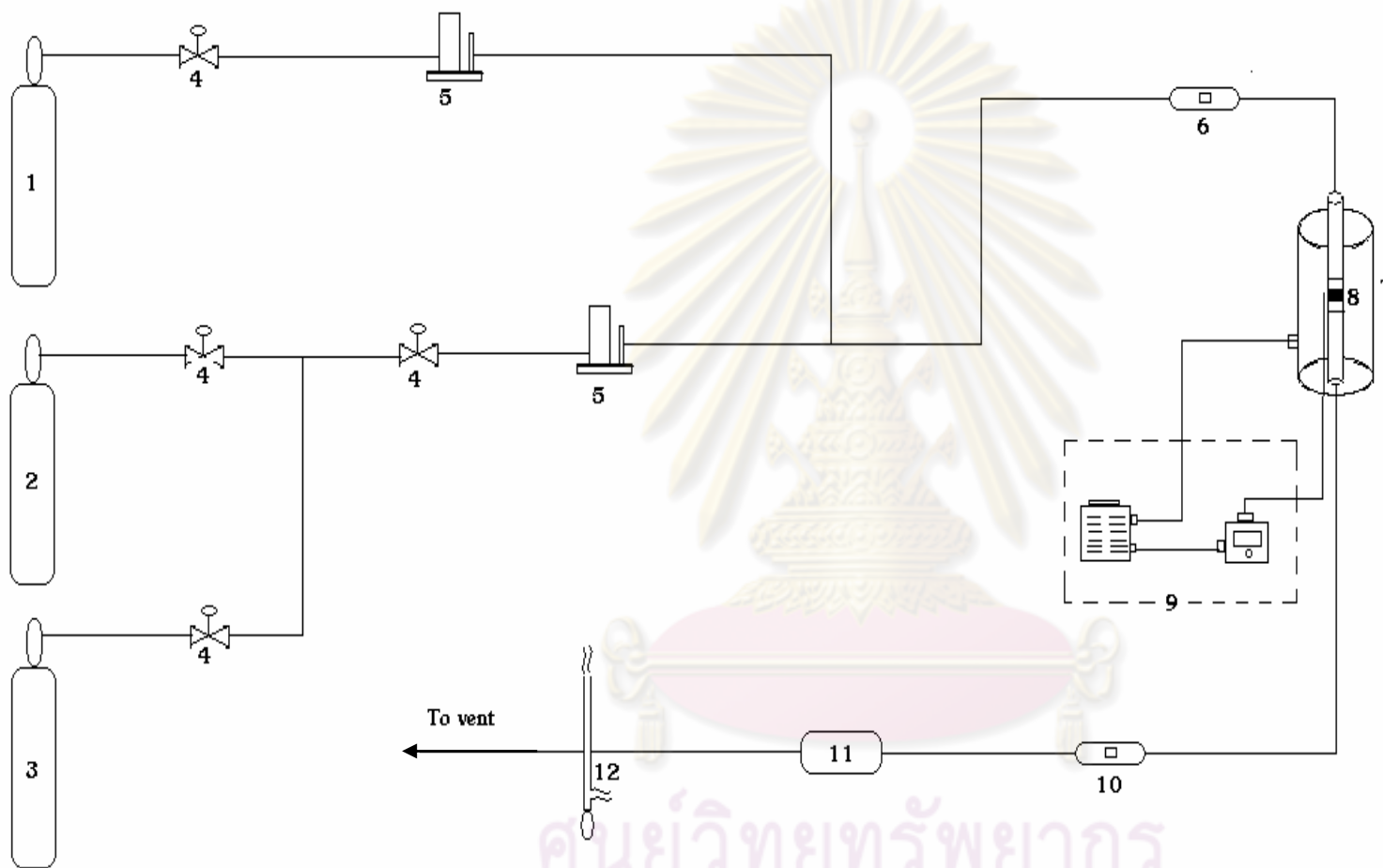
1. 50% CH_4/CO_2 cylinder
2. N_2 cylinder
3. H_2 cylinder
4. Ball valve
5. Mass flow controllers
6. Sampling injection port
7. Furnace
8. Quartz tube fixed bed reactor
9. Temperature controller and variable voltage transformer
10. Gas sample
11. Gas liquid separation

Figure 4.1 Scheme diagram of reforming reaction of methane by CO_2

CHAPTER V

RESULTS AND DISCUSSIONS

This chapter is divided into three sections. The first section contains the effect of phase of alumina on catalytic activity of catalyst. The second section shows effect of supported nickel catalyst on catalytic activity. The last section presents catalytic activity of nickel catalyst on mixed phase of alumina compared with nickel catalyst on silica-magnesium commercial grade.

5.1 The effect phase of alumina supported nickel catalyst on catalytic activity

5.1.1 Characterization of catalyst

This section presents the characterization of supported nickel catalysts. The structure and crystallinity of the catalysts were measured by X-ray diffraction. Scanning electron microscopy was used to study the morphology of the catalysts. The specific surface area was determined by nitrogen physisorption technique. Amount of carbon monoxide adsorbed on nickel catalyst was measured by CO chemisorptions technique which is relative to the amount of active site of nickel catalysts. Transmission electron microscopy was investigated for nickel catalysts after being used in carbon dioxide reforming of methane. The acidity of nickel catalyst measured by Temperature Programmed Desorption of ammonia (NH_3-TPD). Hydrogen Temperature Programmed Reduction (H_2-TPR) was investigated for reducing temperature of nickel catalyst. Amount of coke on nickel catalyst was measured by thermo gravimetric and differential thermal analysis.

5.1.1.1 X-Ray Diffraction

The X-Ray Diffraction patterns for the synthetic mixed phase of alumina by solvothermal methods and commercial γ-Al_2O_3 support are shown in Figure 5.1. The XRD patterns both of commercial γ-Al_2O_3 and synthetic mixed phase of alumina were obvious at 32°, 37°, 39°, 45°, 61° and 66° as pure γ- phase [Meephoka et al. 2008].

At 43° is the position assigned to χ-alumina at which the pure γ-alumina phase does not occur.
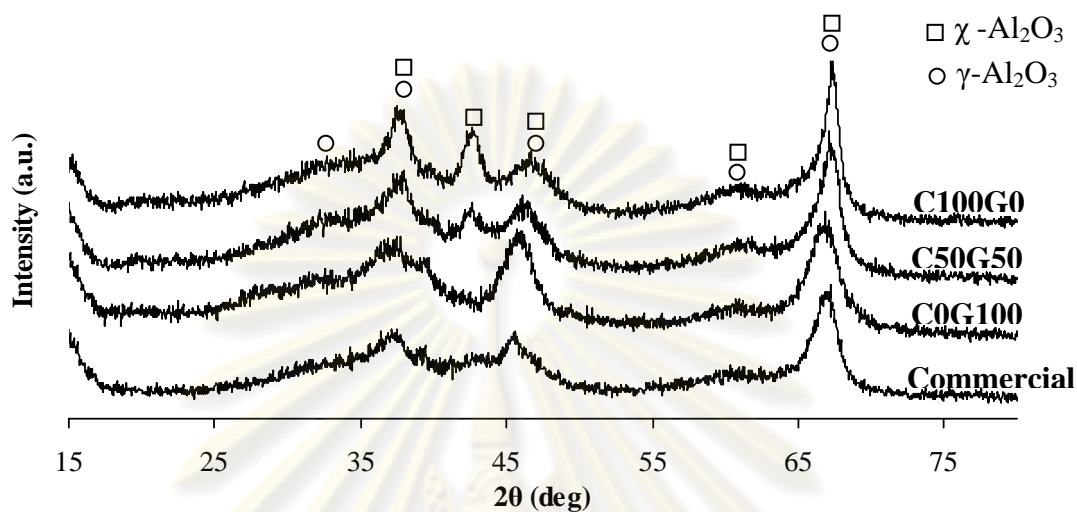

Figure 5.1 XRD patterns of the commercial γ-Al$_2$O$_3$ and synthetic mixed phase of alumina.

Figure.5.2 shows XRD pattern of 7%wt nickel catalyst on synthetic mixed phase of alumina and commercial γ-Al$_2$O$_3$. XRD peak of nickel oxide should occur at 37.3°, 43.4°, 62.9° and 75.3°[Gao, et al. 2008] but non of those peaks was observed probably because of small loading amount of nickel.
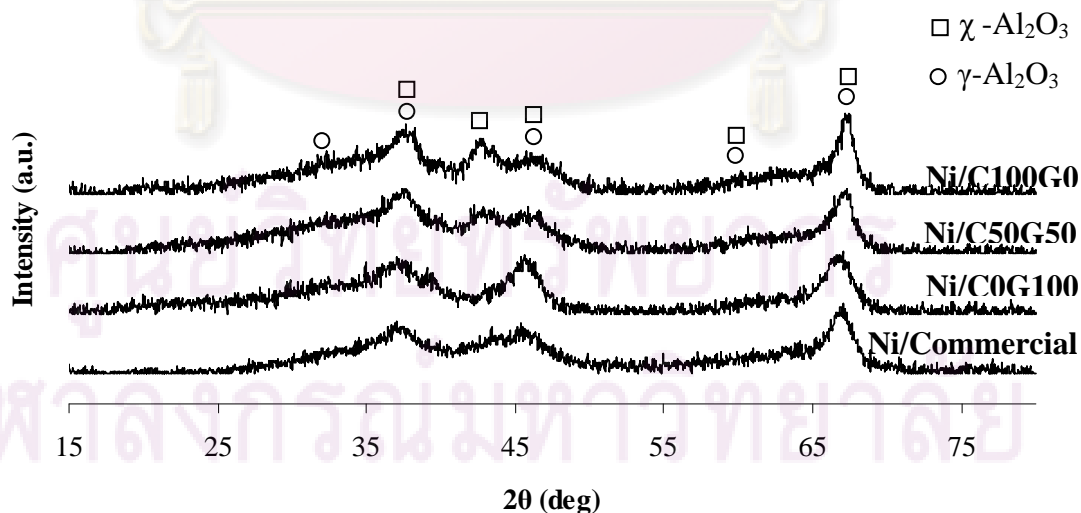

Figure 5.2 XRD patterns of 7%wt nickel catalyst on the commercial γ-Al$_2$O$_3$ and synthetic mixed phase of alumina.

5.1.1.2 Nitrogen physisorption

The specific surface areas of commercial γ-Al$_2$O$_3$, synthetic mixed phase of alumina, and 7%wt nickel catalysts on supported-alumina are determined by BET technique. The results are summarized in Table 5.1. It is found that specific surface area of all supported catalysts decreased with the addition of nickel. Pore volume of the supported catalyst is not different with the addition nickel though the decrease of pore size was found.

Table 5.1 Physical properties of 7% nickel catalysts on supported- alumina.

Catalysts	Specific surface area, m^2/g	Pore volume, cm^3/g	Pore size, (A°)
γ-Al$_2$O$_3$ (com)	149	0.23	37
C0G100-Al$_2$O$_3$	159	0.44	81.4
C50G50-Al$_2$O$_3$	185	0.57	81.8
C100G0-Al$_2$O$_3$	152	0.45	96.5
Ni/ γ-Al$_2$O$_3$ (com)	125	0.20	38.4
Ni/ C0G100-Al$_2$O$_3$	139	0.36	74.5
Ni/ C50G50-Al$_2$O$_3$	160	0.47	73.3
Ni/ C100G0-Al$_2$O$_3$	132	0.45	74.5

5.1.1.3 Ammonia Temperature Programmed Desorption (NH$_3$-TPD)

The NH$_3$-TPD profiles for alumina supported with different wt% of χ-phase contents are shown in Figure 5.3. The profiles are composed of two peaks, i.e. a high temperature peak representing strong acid sites and a low temperature one referring to weak acid sites. It was found that all support showed two broad peaks during the temperature range of 45 to 240°C and 240 to 500°C, respectively. Synthetic pure γ-alumina has the highest acidity than that of among commercial γ-alumina, 50% χ-γ-alumina and pure χ-alumina. The acid properties of the alumina catalysts are also reported in Table 5.2. The calculation of the acidity is shown in Appendix D. The acidity of pure γ- and pure χ-alumina was 17.55 and 10.55 mmol H$^+$/g catalyst,

respectively. The increasing order of total acidity concentration (mmol H^+/g catalyst) is as follows: C0G100> γ-Al$_2$O$_3$ (com) > C50G50 $\approx$ C100G0.
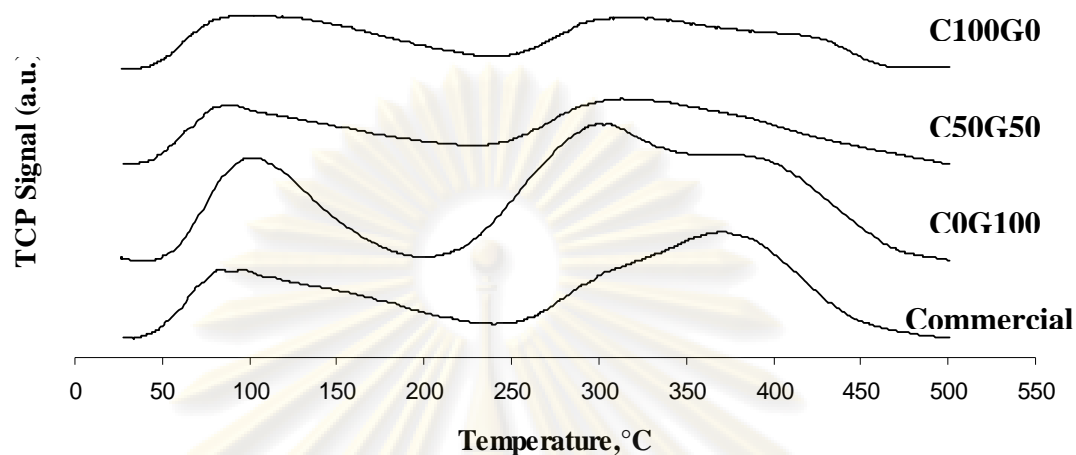

Figure 5.3 The NH$_3$-TPD profile of synthetic alumina and commercial γ-Al$_2$O$_3$.

Table 5.2 Acidity of commercial γ-Al$_2$O$_3$ and synthetic alumina supported.

Catalysts	Adsorbed volume of ammonia, (ml)	Total acid site, (mmol H^+/g)
γ-Al$_2$O$_3$ (com)	27.15	11.0578
C0G100-Al$_2$O$_3$	43.40	17.5556
C50G50-Al$_2$O$_3$	25.69	10.3735
C100G0-Al$_2$O$_3$	26.16	10.5510

The NH$_3$-TPD profiles for 7%wt. supported nickel catalyst with different phase of support are shown in Figure 5.4. The profiles are composed of two peaks, i.e. a high temperature peak representing strong acid sites and a low temperature one referring to weak acid sites. It was found that all support showed two broad peaks during the temperature range of 45 to 240°C and 240 to 500°C, respectively. Synthetic pure γ-alumina has the highest acidity than that of among commercial γ-alumina, 50% χ-γ-alumina and pure χ-alumina. The acid properties of the alumina catalysts are also reported in Table 5.3. The calculation of the acidity is shown in Appendix D. The acidity of pure γ- and pure χ-alumina was 10.57 and 10.44 mmol

H$^+$/g catalyst, respectively. The increasing order of total acidity concentration (mmol H$^+$/g catalyst) is as follows: C50G50>C0G100 ≈ C100G0> γ-Al$_2$O$_3$ (com).
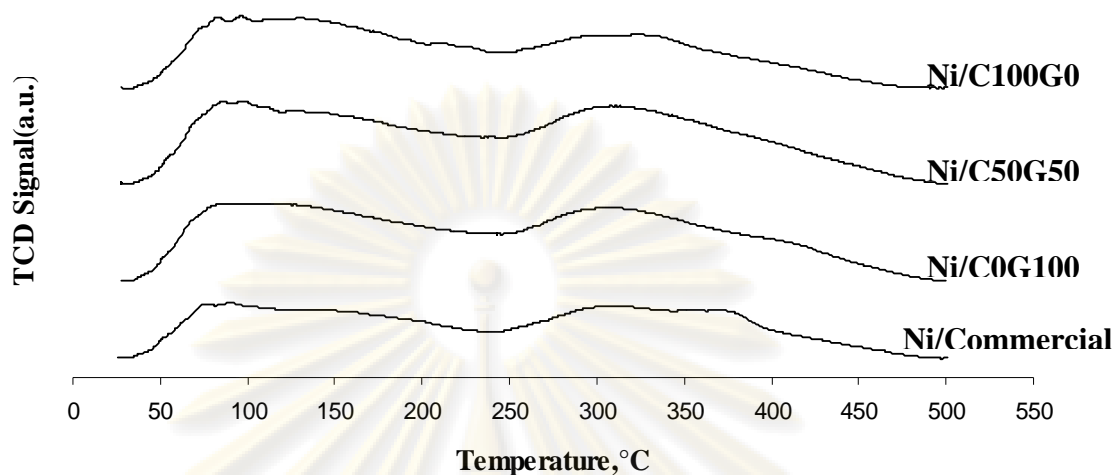

Figure 5.4 The NH$_3$-TPD profile of 7%wt.nickel catalyst on synthetic alumina and commercial γ-Al$_2$O$_3$.

Table 5.3 Acidity of 7%wt.Ni catalyst on commercial γ-Al$_2$O$_3$ and synthetic alumina.

Catalysts	Adsorbed volume of ammonia, (mL)	Total acid site, (mmol H$^+$/g)
Ni/ γ-Al$_2$O$_3$ (com)	19.16	7.81
Ni/ C0G100-Al$_2$O$_3$	26.20	10.57
Ni/ C50G50-Al$_2$O$_3$	29.76	12.15
Ni/ C100G0-Al$_2$O$_3$	25.54	10.44

5.1.1.4 CO-chemisorption

Active site of catalysts can be determined by calculation from amount of carbon monoxide adsorption on catalysts. The calculation the active site of catalysts is shown in Appendix C. Absorbed amount of carbon monoxide is directly proportional to the active site, i.e. the higher absorbed amount of carbon monoxide means the higher active site. From Table 5.4, mixed phase between 50% χ -γ- alumina has the highest active site. Amount of active site of pure χ-alumina has higher active site than that of pure γ-alumina. A nickel catalyst on synthetic mixed phase of alumina has

higher active site than that of commercial γ-Al_2O_3. The crystallite size and percent dispersion of nickel catalyst can be determined by calculation from amount of carbon monoxide adsorption on catalysts that shown in Appendix C. The nickel catalyst on synthetic alumina support has higher dispersed than that of commercial γ-Al_2O_3. The crystallite size of nickel catalyst on synthetic alumina has smaller than that of commercial γ-Al_2O_3. The data of crystallite size and percent dispersion of nickel catalyst is shown in Table 5.4.

Table 5.4 showed amount of carbon monoxide adsorbed on catalysts.

Catalysts	Active site, Molecule*10^{-18} per gram	% dispersion of nickel	Crystallite size of Ni, nm
Ni/ γ-Al_2O_3 (com)	20.16	0.32	322.96
Ni/ C0G100-Al_2O_3	14.35	2.28	44.80
Ni/ C50G50-Al_2O_3	34.90	2.67	38.35
Ni/ C100G0-Al_2O_3	23.95	3.86	26.54

5.1.1.5 Hydrogen Temperature Programmed Reduction (H$_2$-TPR)

H$_2$-TPR pattern of nickel catalysts on support are shown in Figure.5.5. The reduction peak of free NiO species occurs at 400 ℃, which have weak interaction with support. That showed nickel catalyst on alumina is NiO species. The reduction peak of complex NiO$_x$ species will occur at above 800 ℃ and NiAl$_2$O$_4$ will occur at above 900 ℃ [Koo et al., 2008], which both species did not occur for nickel catalyst in this research.
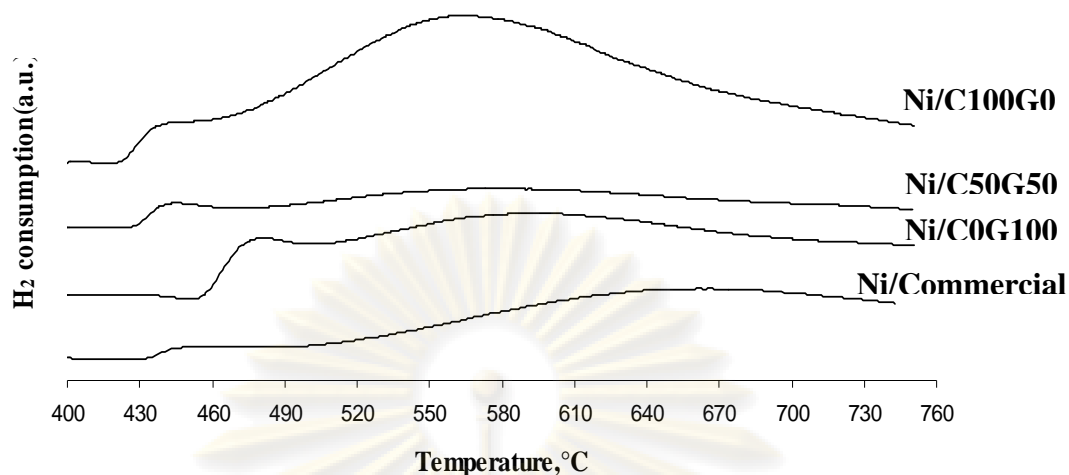
Figure 5.5 H_2-TPR patterns of Ni/Al_2O_3 catalysts with various alumina phases.

5.1.2 Reaction study for commercial γ-Al_2O_3 and synthetic Al_2O_3 supported nickel catalysts

Figure 5.6 presents comparison of methane conversion for reforming reaction of methane by carbon dioxide over nickel catalyst on synthetic alumina and commercial γ-alumina. All catalysts at initial time exhibited the methane conversion of about 81-82% except that the conversion of nickel catalyst on commercial γ-alumina was 78%. All catalysts at final time exhibited the conversion of methane of about 82-84% except that the conversion of nickel catalyst on commercial γ-alumina was 70%. The nickel catalyst on 50%χ-γ- alumina gave the highest methane conversion of about 84%, while those of nickel catalyst on pure χ-alumina, pure γ-alumina, and commercial γ-alumina were approximately 80%, 75%, and 69%, respectively.
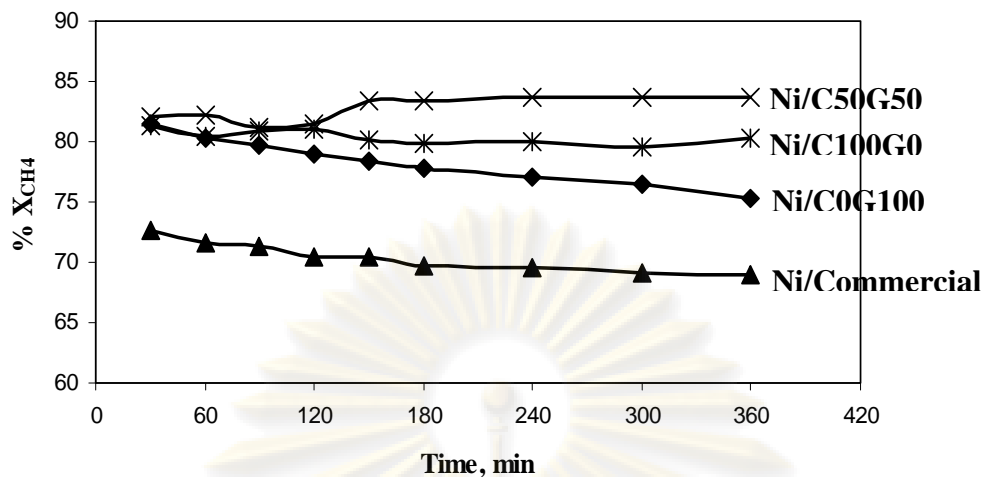
Figure 5.6 The effect of supported-nickel catalyst on the CH$_4$ conversion.

Figure 5.7 presents comparison of carbon dioxide conversion for reforming reaction of methane by carbon dioxide over nickel catalyst on synthetic alumina and commercial γ-alumina. Nickel catalysts on 50%χ-γ- alumina at initial time exhibited the carbon dioxide conversion of about 88%, while those of nickel catalyst on pure χ-alumina, pure γ-alumina, and commercial γ-alumina were approximately 84%, 85%, and 68%, respectively. The nickel catalyst on 50%χ-γ- alumina gave the highest methane conversion of about 88%, while those of nickel catalyst on pure χ-alumina, pure γ-alumina, and commercial γ-alumina were approximately 82%, 76%, and 63%, respectively.
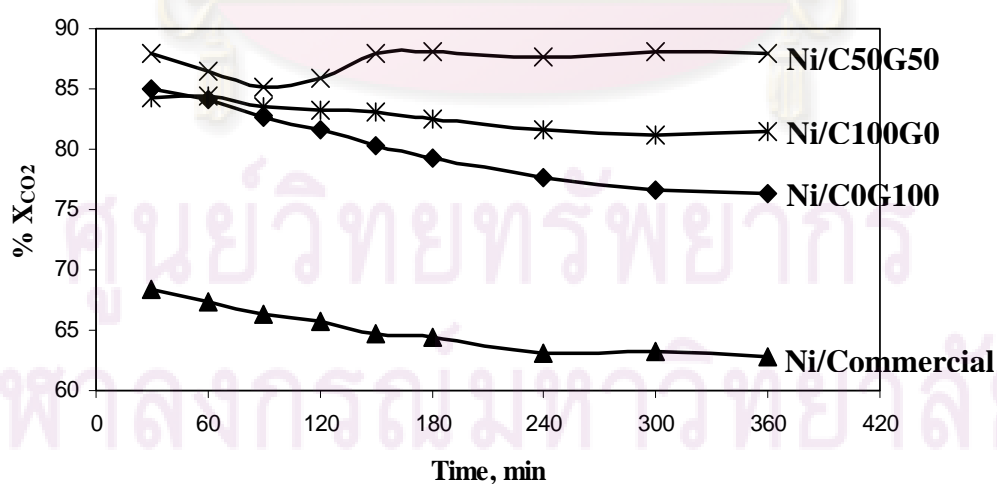

Figure 5.7 The effect of supported-nickel catalyst on the CO$_2$ conversion.

The catalytic activity of nickel catalysts on synthetic alumina relates directly with the active site. The commercial γ-alumina has higher active site than that of synthetic pure γ- alumina, but having less catalytic activity than synthetic pure γ-alumina. This may be due to the pore volume and pore size of commercial γ-alumina which is less than that of pure γ-alumina, resulting in less adsorption of reactant.

When compared between methane conversion and carbon dioxide conversion, it was found that the carbon dioxide conversion was higher than that of methane conversion. This indicates that further carbon dioxide was consumed in another reaction such as a reverse water gas shift reaction.

5.1.2.1 Morphology

The morphology characterized by Scanning Electron Microscopy (SEM). Figure.5.8-5.11 shows the SEM images of fresh catalyst and used catalysts. A lot more filament carbon species was observed on used catalyst.
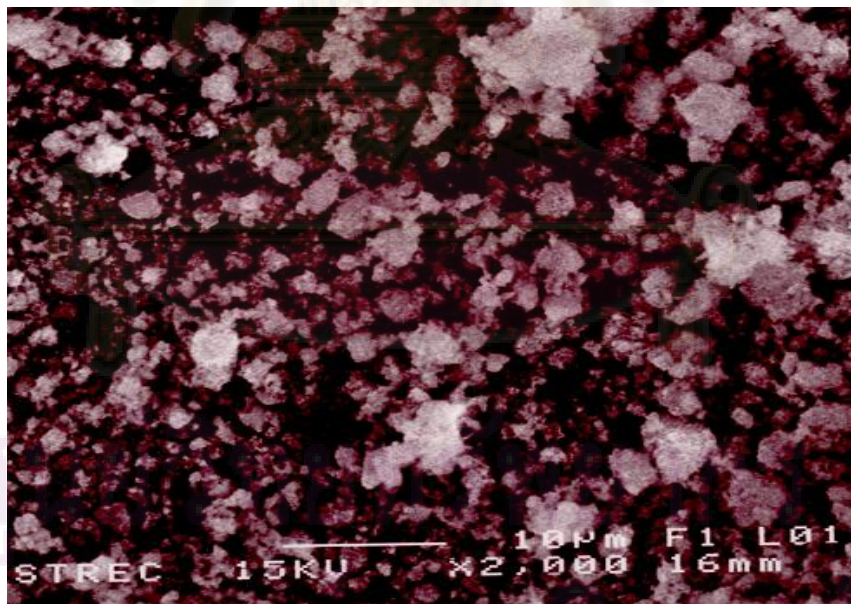

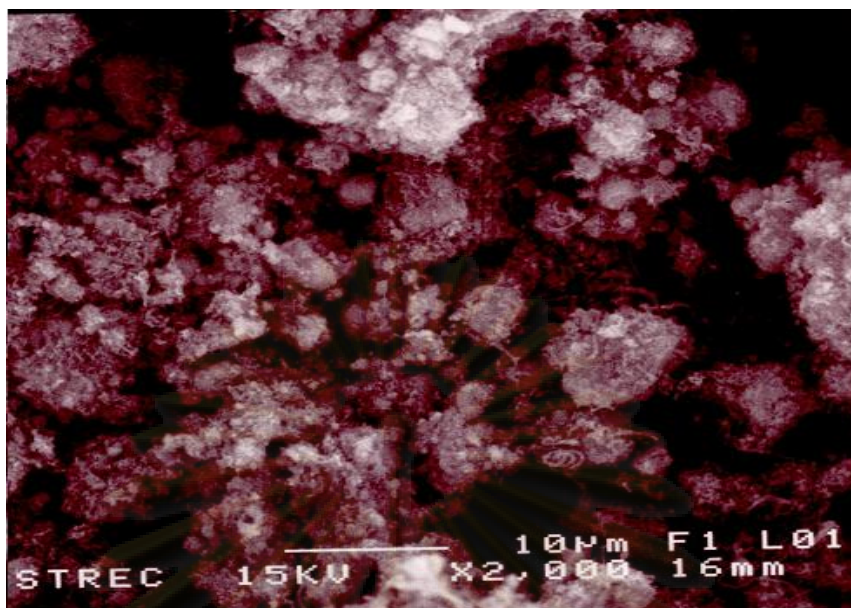**Figure 5.8** (a) The SEM images showed fresh Ni/C0G100 catalyst.

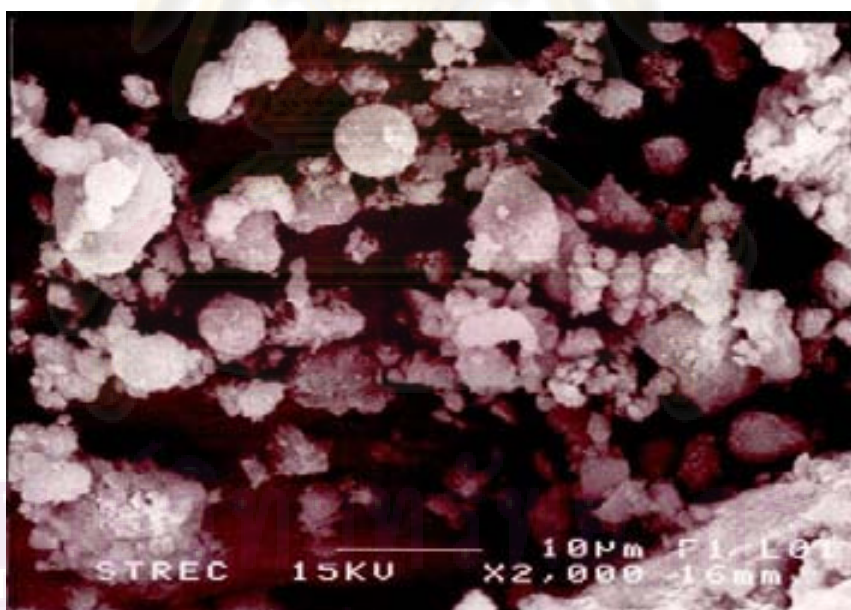**Figure 5.8** (b) The SEM images showed used Ni/C0G100 catalyst.

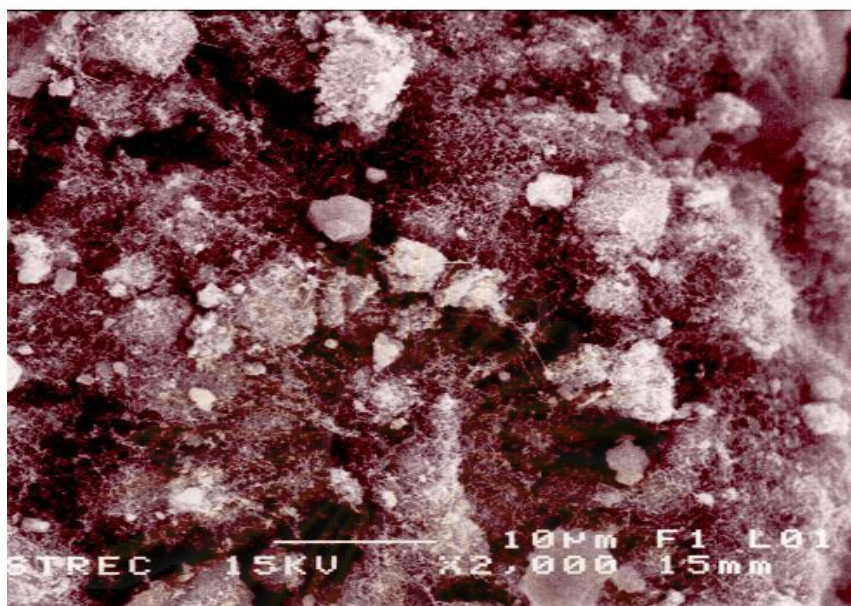**Figure 5.9** (a) The SEM images showed fresh Ni/C50G50 catalyst.

Figure 5.9 (b) The SEM images showed used Ni/C50G50 catalyst.
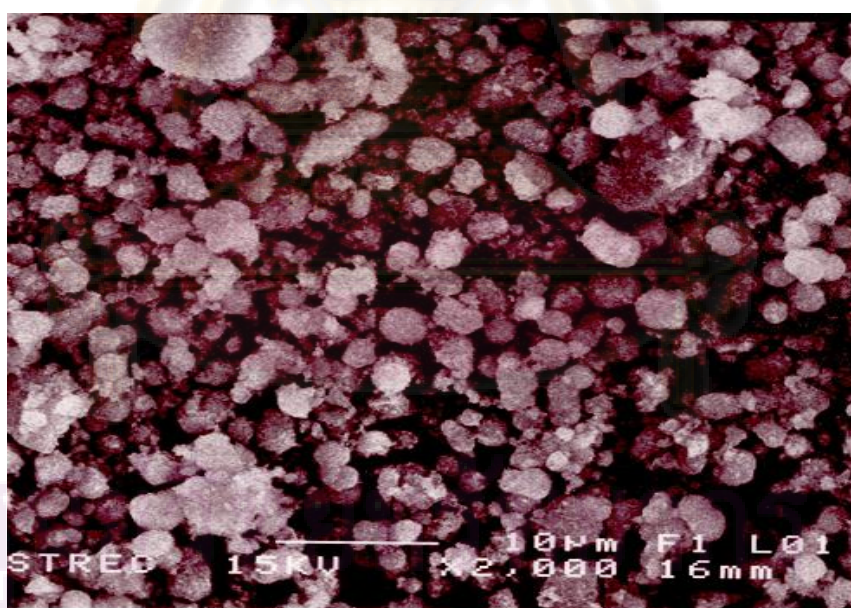

Figure 5.10 (a) The SEM images showed fresh Ni/C100G0 catalyst.

Figure 5.10 (b) The SEM images showed used Ni/C100G0 catalyst.

Figure 5.11 (a) The SEM images showed fresh Ni/ γ- Al_2O_3 commercial catalyst.
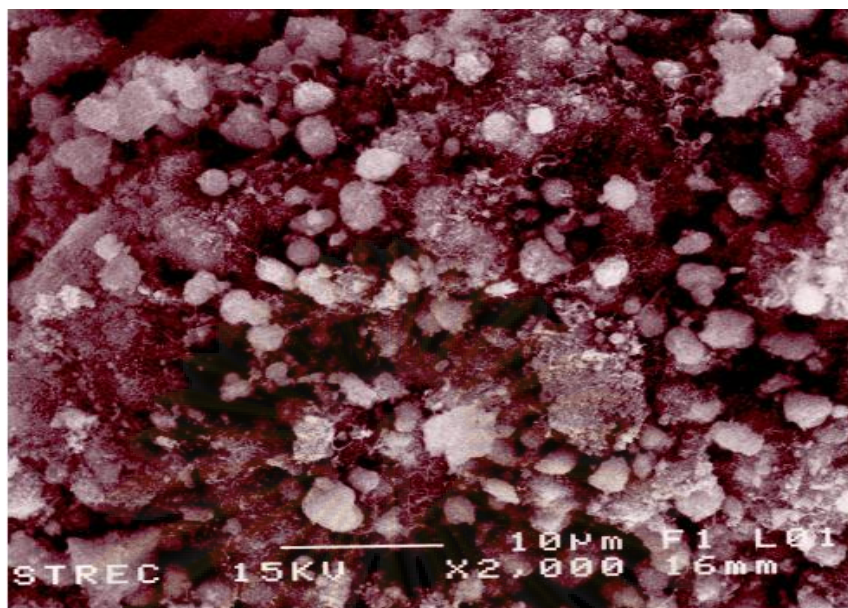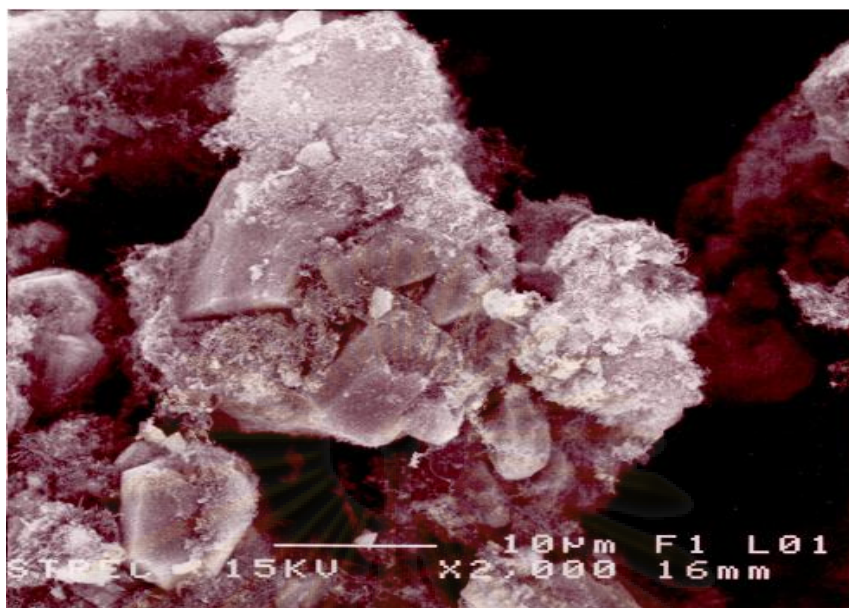
Figure 5.11 (b) The SEM images showed used Ni/ γ- Al$_2$O$_3$ commercial catalyst.

The used catalysts were then characterized by TEM techniques to investigate filamentous carbon on the catalysts.

5.1.2.2 Transmission Electron Microscope (TEM)

Figure.5.12 showed used catalysts characterized by TEM techniques. The filamentous carbon found was long hollow filament with possibly nickel particle at filament tip. This supposed to be whisker coke which does not affect the catalytic activity, but results in a pressure drop due to reactor blockage. [Koo et al., 2008]
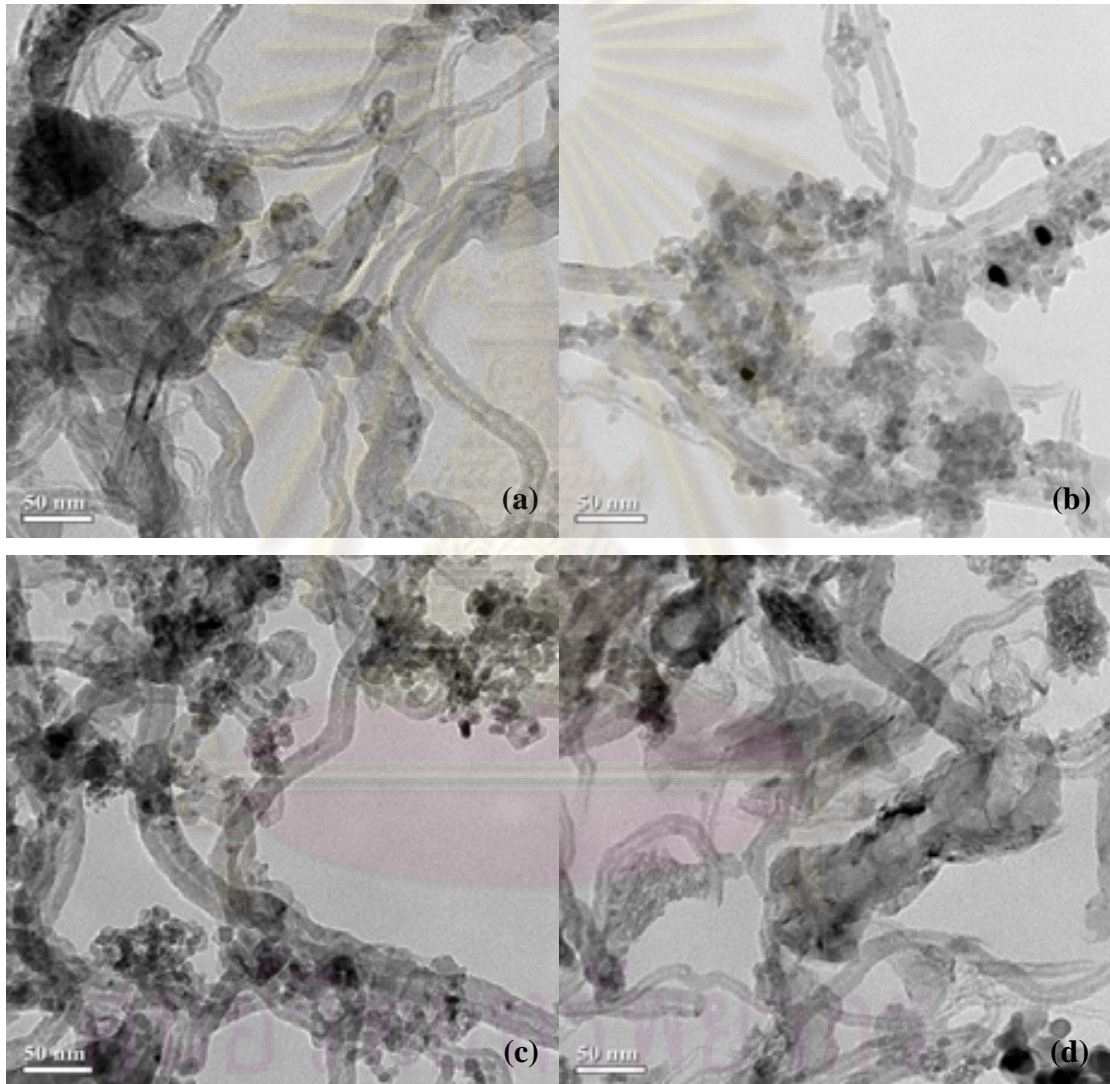

Figure 5.12 The TEM images showed filamentous carbon on used nickel catalysts (a) C0G100, (b) C50G50, (c) C100G0, (d) γ- Al_2O_3 commercial.

5.1.2.3 Amount of coke

Amount of coke was characterized by Thermogravimetric and differential thermal analysis (TG-DTA). When compared the percent conversion difference of methane and carbon dioxide ($\%X_{CO2}-\%X_{CH4}$) of each catalysts, it has been found that the decreasing order of feed conversion difference was as follow: 50%χ-γ- alumina, pure χ- alumina, pure γ- alumina, and commercial γ- alumina, respectively. That showed this reaction give water as byproduct. Amount of water relates directly to the conversion difference of carbon dioxide and methane. Figure.5.13 showed percent weight loss versus temperature which found that all catalysts contain weight loss during the temperature of 400-600 ℃. Koo and co-worker (2008) has reported that corresponds to the coke decomposition on catalyst surface.
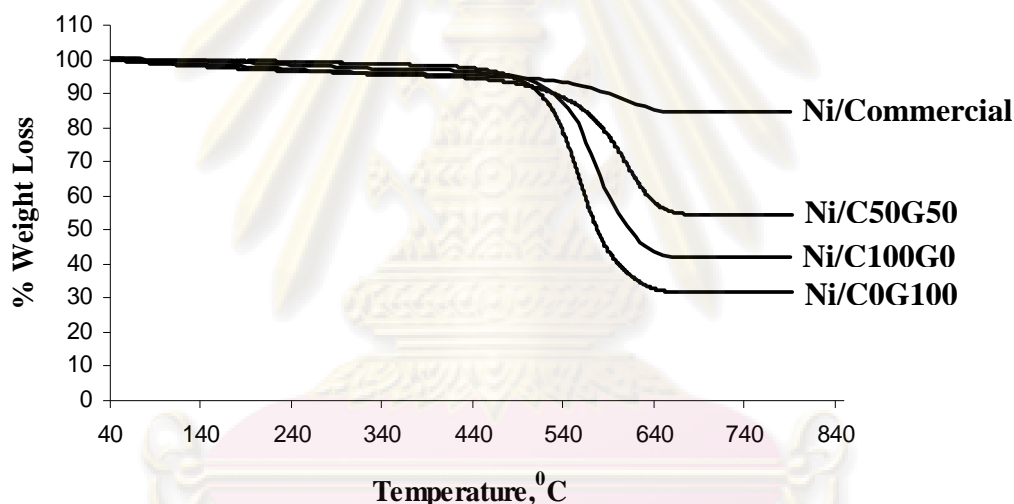

Figure 5.13 TG profiles of used 7 wt. % nickel catalysts on support under air.

It was found that the mixed phase of alumina contains smallest weight loss compared with nickel catalyst on pure χ-alumina and pure γ-alumina. The small percent weight loss means less amount of coke. A nickel catalyst on pure γ-alumina support contains more percent weight loss than that of pure χ-alumina. The conversion difference of carbon dioxide and methane reflects the amount of water occurred in the side reaction of carbon dioxide such as reverse water gas shift reaction. In the presence of such water, the coke formation on catalyst tends to be prevented via the reaction as follows:

$$C_{ads} + H_2O \rightarrow CO + H_2 \qquad \Delta H^o_{298} = 131.4 \ kJ/mol$$
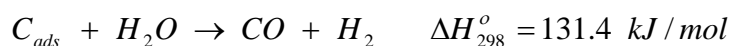
5.2 The effect ratio of Si/Al of zeolite Y supported nickel catalyst on catalytic activity

5.2.1 Characterization of catalyst

5.2.1.1 X-Ray Diffraction

The X-ray diffraction patterns commercial zeolite Y (Si/Al ratio=7, and 200) are shown in Figure 5.14. The XRD patterns both of commercial zeolite Y (Si/Al =7, and 200) were obvious at 10.5°, 12.2°, 15.9°, 23.9°, 27.5°, 31.4°, 32.0°, and 34.8° as zeolite Y [Halliche et. al, 2005].
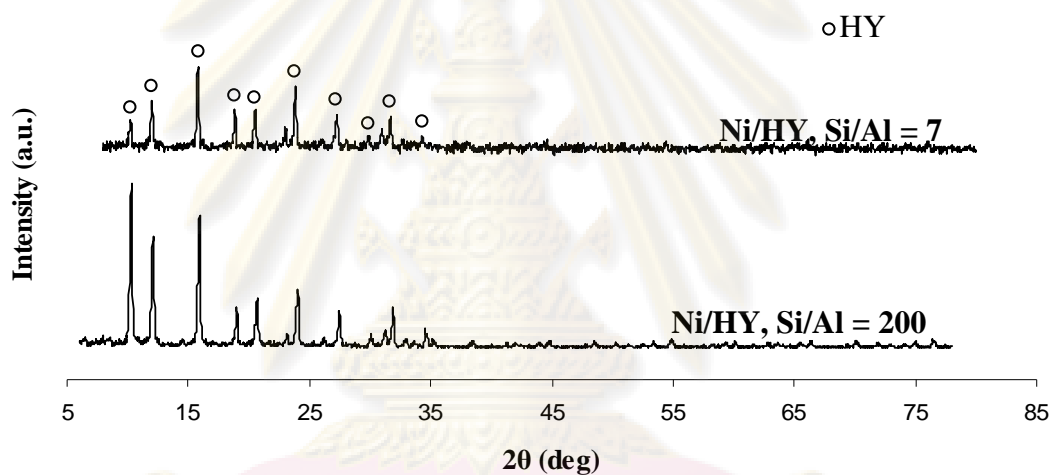

Figure 5.14 XRD patterns of the commercial zeolite Y.

Figure.5.15 shows XRD pattern of 7%wt nickel catalyst on commercial zeolite Y. XRD peak of nickel oxide should occur at 37.3°, 43.4°, 62.9° and 75.3°[Gao et. al, 2008] but non of those peaks was observed probably because of small loading amount of nickel.
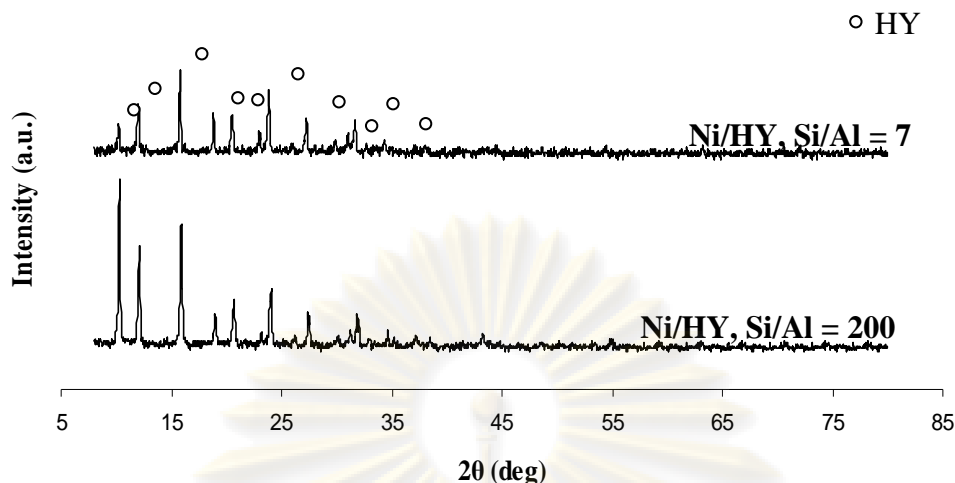
Figure 5.15 XRD patterns of 7%wt nickel catalyst on commercial zeolite Y.

5.2.1.2 Nitrogen physisorption

The specific surface areas of commercial zeolite Y (Si/Al ratio = 7, 200), and 7%wt nickel catalysts on commercial zeolite Y are determined by BET technique. The results are summarized in Table 5.5. It is found that specific surface area of all supported catalysts decreased with the addition of nickel. Pore volume and pore size of the supported catalyst is decrease with the addition nickel.

Table 5.5 Physical properties of 7% nickel catalysts on supported- zeolite Y.

Catalysts	Specific surface area, m^2/g	Pore volume, cm^3/g	Pore size, (A°)
HY, Si/Al = 7	728	0.25	72.3
HY, Si/Al = 200	617	0.21	69.0
Ni/HY, Si/Al = 7	603	0.10	52.3
NiHY, Si/Al = 200	522	0.08	59.2

5.2.1.3 Ammonia temperature-programmed desorption (NH$_3$-TPD)

The NH$_3$-TPD profiles for commercial zeolite Y with different of Si/Al ratio is 7 and 200 are shown in Figure 5.16 and 5.17, respectively. The profiles are composed of two peaks, i.e. a high temperature peak representing strong acid sites and a low temperature one refering to weak acid sites. Figure 5.16 was found that Si/Al ratio = 7 showed one broad peaks during the temperature range of 40 to 450°C. Figure 5.17 was found that Si/Al ratio = 200 showed one shaft peak and one broad peak during the temperature range of 40 to 150°C and 150 to 450°C. The acid properties of the alumina catalysts are also reported in Table 5.6. The calculation of the acidity is shown in Appendix D. The acidity of Si/Al ratio = 7 and 200 was 20.25 and 11.85 mmol H$^+$/g catalyst, respectively.
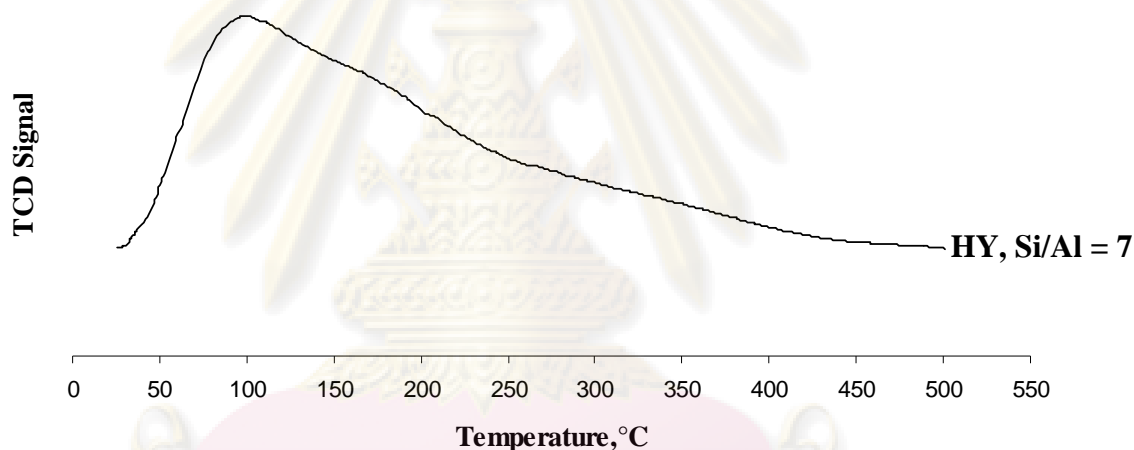

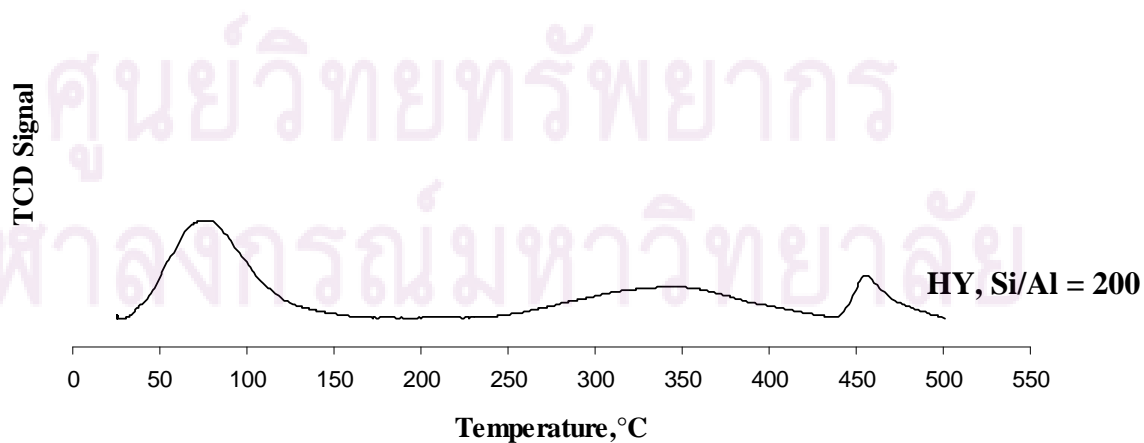**Figure 5.16** The NH$_3$-TPD profile of commercial zeoliteY, Si/Al = 7.

Figure 5.17 The NH$_3$-TPD profile of commercial zeoliteY.

Table 5.6 Acidity of commercial zeoliteY.

Catalysts	Adsorbed volume of ammonia, (mL)	Total acid site, (mmol H^+/g)
HY, Si/Al = 7	49.86	20.25
HY, Si/Al = 200	29.00	11.85

The NH_3-TPD profiles for supported 7%wt.nickel catalyst with different Si/Al ratio is 7 and 200 are shown in Figure 5.18 and 5.19, respectively. The profiles are composed of two peaks, i.e. a high temperature peak representing strong acid sites and a low temperature one refering to weak acid sites. Figure 5.18 was found that Si/Al ratio = 7 supported catalyst showed one shaft peak and one broad peak during the temperature range of 40 to 250°C and 250 to 500°C, respectively. Figure 5.19 was found that Si/Al ratio = 200 supported catalyst showed one shaft peak and one broad peak during the temperature range of 40 to 180°C and 230 to 500°C. The acid properties of the alumina catalysts are also reported in Table 5.7. The calculation of the acidity is shown in Appendix D. The acidity of Si/Al ratio = 7 and 200 was 45.41 and 25.80 mmol H^+/g catalyst, respectively.
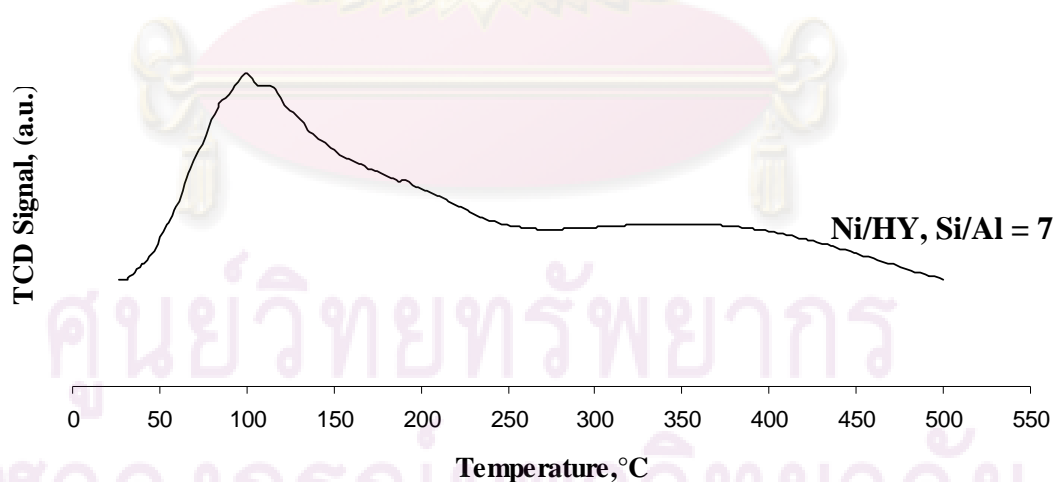

Figure 5.18 The NH_3-TPD profile of 7%wt.nickel catalyst on commercial zeoliteY, Si/Al=7.
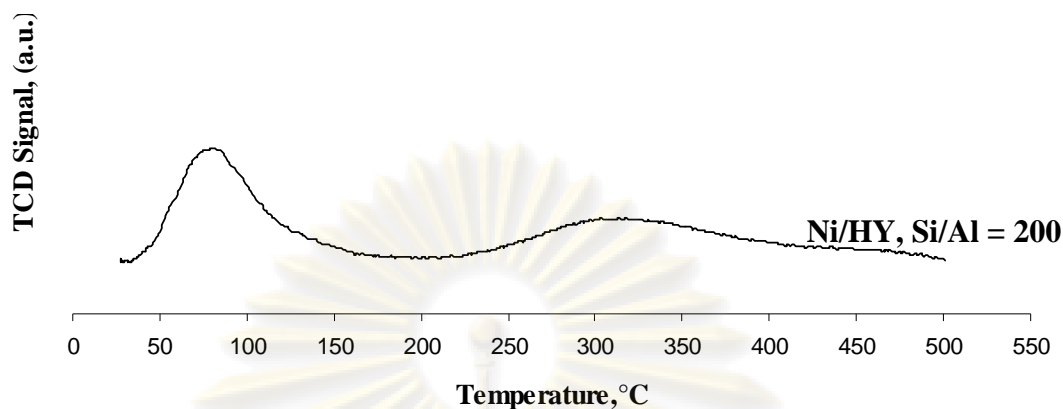
Figure 5.19 The NH$_3$-TPD profile of 7%wt.nickel catalyst on commercial zeoliteY, Si/Al=200.

Table 5.7 Acidity of 7%wt.Ni catalyst on commercial zeoliteY.

Catalysts	Adsorbed volume of ammonia, (mL)	Total acid site, (mmol H$^+$/g)
Ni/HY, Si/Al = 7	113.03	45.41
NiHY, Si/Al = 200	63.15	25.80

5.2.1.4 CO-chemisorption

Active site of catalysts can be determined by calculation from amount of carbon monoxide adsorption on catalysts. Absorbed amount of carbon monoxide is directly proportional to the active site, i.e. the higher absorbed amount of carbon monoxide means the higher active site. From Table 5.8, zeolite Y Si/Al ratio=7 has the higher active site than that of Si/Al ratio=200. The Crystallite size and percent dispersion of nickel catalyst can be determined by calculated from amount of carbon monoxide adsorption on catalysts that shown in Appendix C. The nickel catalyst on Si/Al ratio=200 of zeolite Y has higher dispersed than that of Si/Al ratio=7 of zeolite Y. The crystallite size of nickel catalyst on Si/Al ratio=200 of zeolite Y has smaller

than that of Si/Al ratio=7 of zeolite Y. The data of crystallite size and percent dispersion of nickel catalyst is shown in Table 5.8.

Table 5.8 showed amount of carbon monoxide adsorbed on catalysts.

Catalysts	Active site, Molecule*10^-18 per gram	% dispersion of nickel	Crystallite size of Ni, nm
Ni/HY, Si/Al = 7	5.39	0.86	119.18
NiHY, Si/Al = 200	8.16	1.30	78.76

5.2.1.5 Hydrogen Temperature Programmed Reduction (H_2-TPR)

H_2-TPR pattern of nickel catalysts on support are shown in Figure.5.20. The reduction peak of free NiO species occurs at 400 ℃, which have weak interaction with support. That showed nickel catalyst on alumina is NiO species. The reduction peak of complex NiO_x species will occur at above 800 ℃ which this species did not occur for nickel catalysts in this research. Based on the TPR profiles, it indicated that nickel oxide dispersed on the Si/Al ratio=200 of zeolite Y exhibited the lower maximum reduction temperature than that of Si/Al ratio=7 of zeolite Y support.
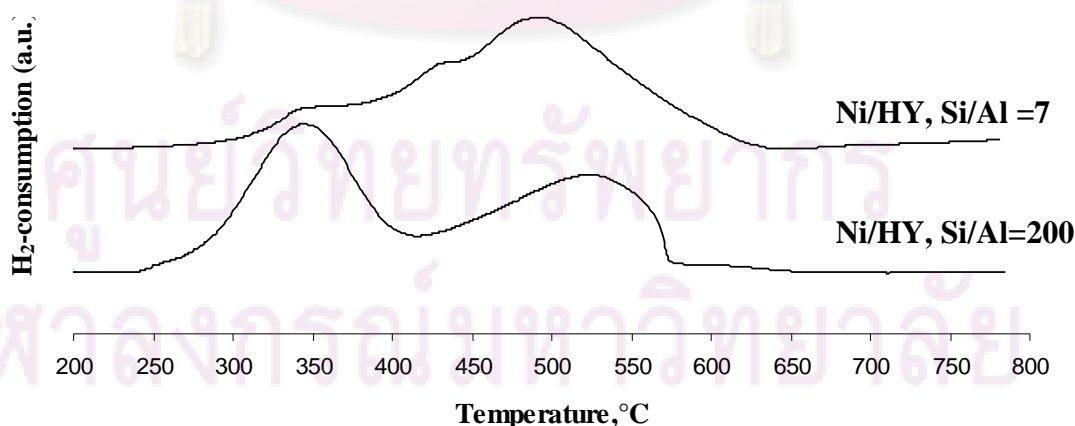

Figure 5.20 H_2-TPR pattern of Ni/zeolite Y catalysts with various Si/Al ratios.

5.2.2 Reaction study for ratio of Si/Al of zeolite Y supported nickel catalyst on catalytic activity

Table 5.9 presents comparison of methane and carbon dioxide conversion for reforming reaction of methane by carbon dioxide over nickel catalyst on commercial zeolite Y (Si/Al ratio=7, 200). The nickel catalyst on Si/Al ratio=200 gave the higher methane conversion and carbon dioxide than that of Si/Al ratio=7. Nickel catalyst on Si/Al ratio=7, and Si/Al ratio=200 were approximately 81%, and 27%, respectively for methane conversion. Nickel catalyst on Si/Al ratio=7, and Si/Al ratio=200 were approximately 31%, and 79%, respectively for carbon dioxide conversion.

Table 5.9 showed percent conversion of 7%Ni catalyst on zeolite Y supported.

Time, min	Ni/HY, Si/Al=7		Ni/HY, Si/Al=200	
	%X_{CH4}	%X_{CO2}	%X_{CH4}	%X_{CO2}
30	27	31	81	79
60	27	29	82	78
90	25	28	-	-
120	25	28	-	-
150	24	27	-	-
180	24	27	-	-

The catalytic activity of nickel catalysts on commercial zeolite Y various Si/Al ratio relates directly with the active site. The Si/Al ratio=200 has higher active site than that of Si/Al ratio=7.

5.2.2.1 Morphology

The morphology characterized by Scanning Electron Microscopy (SEM). Figure.5.21-5.22 shows the SEM images of fresh catalyst and used catalysts. A lot more filament carbon species was observed on used catalyst.
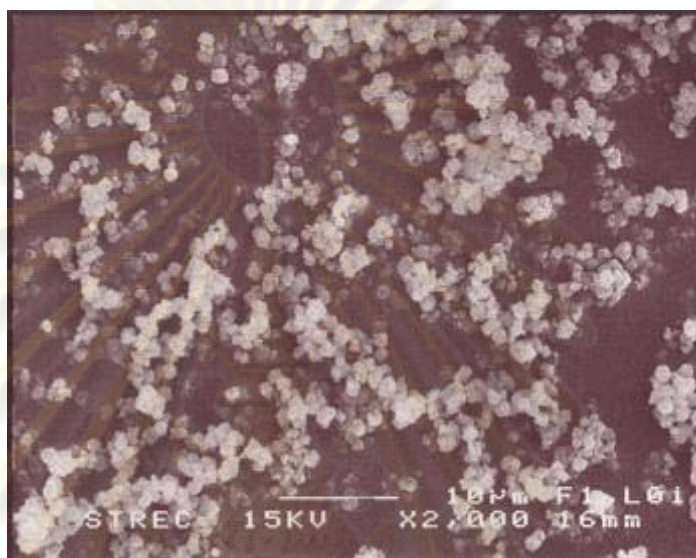

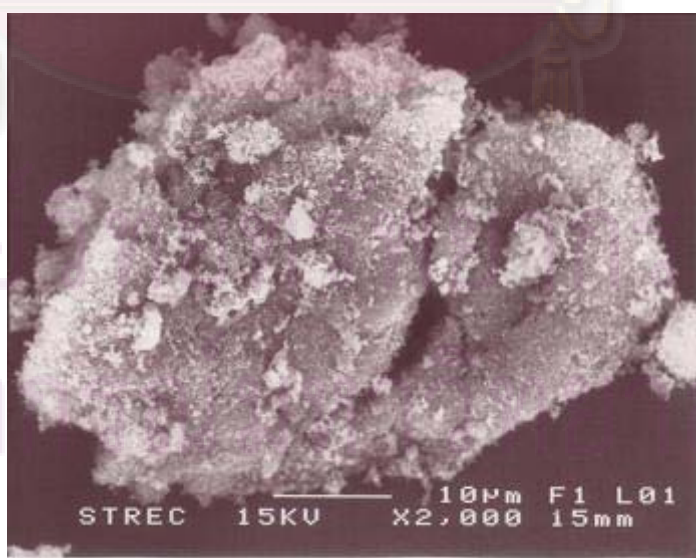**Figure 5.21** (a) The SEM images showed fresh Ni/HY (Si/Al=7) catalyst.

Figure 5.21 (b) The SEM images showed used Ni/ HY (Si/Al=7) catalyst.
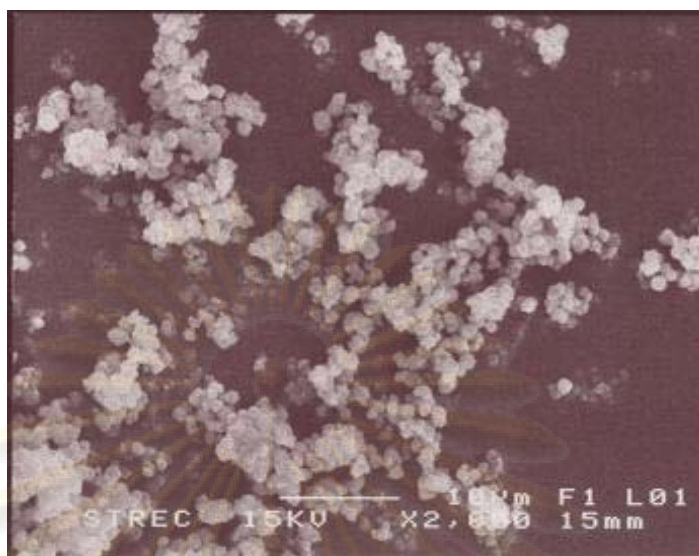
Figure 5.22 (a) The SEM images showed fresh Ni/ HY (Si/Al=200) catalyst.
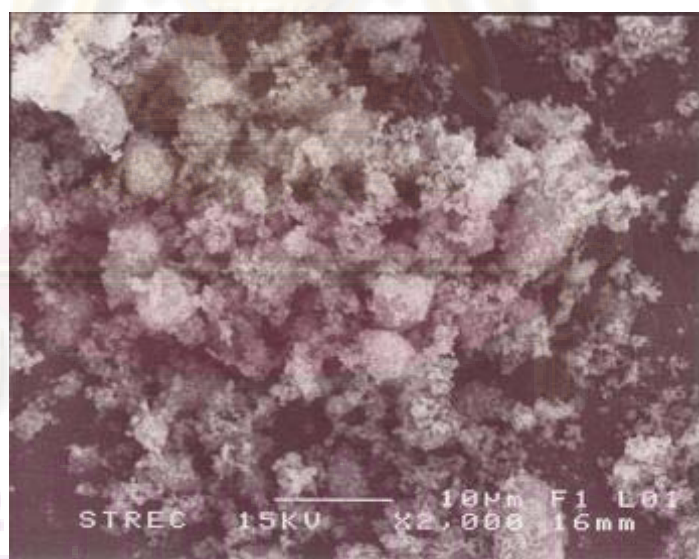

Figure 5.22 (b) The SEM images showed used Ni/ HY (Si/Al=200) catalyst.

The used catalysts were then characterized by TEM techniques to investigate filamentous carbon on the catalysts.

5.2.2.2 Transmission Electron Microscope (TEM)

Figure.5.23 showed used catalysts characterized by TEM techniques. The filamentous carbon found was long hollow filament with possibly nickel particle at filament tip. This supposed to be whisker coke which does not affect the catalytic activity, but results in a pressure drop due to reactor blockage. [Koo et. al, 2008].
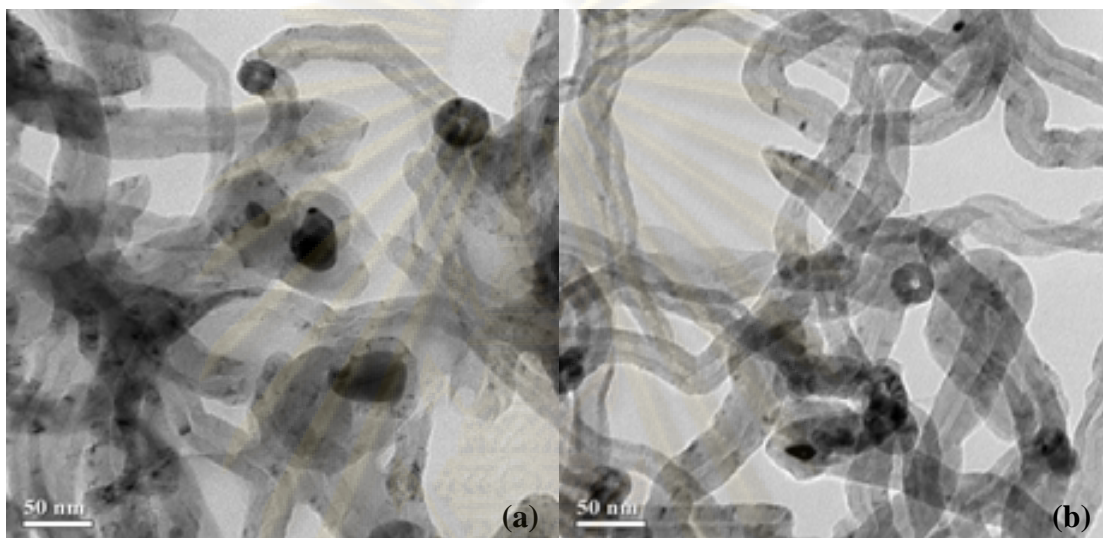

Figure 5.23 The TEM images showed filamentous carbon on used nickel catalysts (a) Si/Al=7, (b) Si/Al=200

5.2.2.3 Amount of coke

Amount of coke was characterized by Thermogravimetric and differential thermal analysis (TG-DTA). When compared between methane conversion and carbon dioxide conversion, it was found that the carbon dioxide conversion was higher than that of methane conversion for Si/Al ratio=7. This indicates that further carbon dioxide was consumed in another reaction such as a reverse water gas shift reaction. That showed this reaction give water as byproduct. Amount of water relates directly to the conversion difference of carbon dioxide and methane. Figure.5.24 showed percent weight loss versus temperature which found that all catalysts contain weight loss during the temperature of 400-600 ℃. Koo and co-worker (2008) has reported that corresponds to the coke decomposition on catalyst surface.
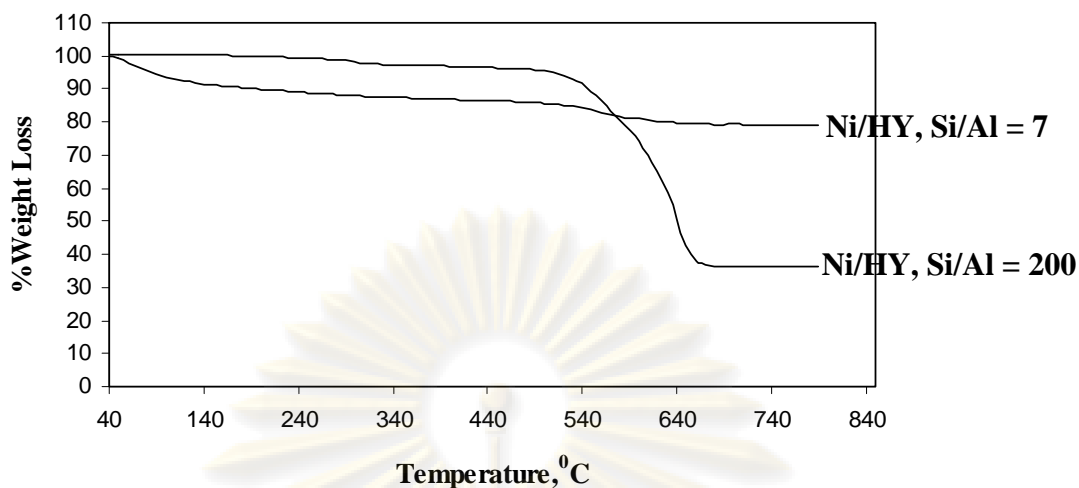
Figure 5.24 TG profiles of used 7 wt. % nickel catalysts on support under air.

It was found that the nickel catalyst on HY Si/Al=7 contains have smaller weight loss compared with nickel catalyst on HY Si/Al=7. The small percent weight loss means less amount of coke. Nickel catalysts on HY Si/Al=7 has smaller contains more percent weight loss than that of HY Si/Al=7. The conversion difference of carbon dioxide and methane reflects the amount of water occurred in the side reaction of carbon dioxide such as reverse water gas shift reaction.

5.3 Catalytic activity of nickel catalyst on mixed phase of alumina compared with nickel catalyst on silica-magnesium commercial grade

5.3.1 Characterization of catalyst

5.3.1.1 X-Ray Diffraction

The X-ray diffraction patterns commercial Ni/SiO_2-MgO are shown in Figure 5.25. The XRD patterns both of commercial Ni/SiO_2-MgO were occured at 18.6°, 32.9, 38.1°, 50.9°, 58.7°, and 62.1° as MgO [Aramendia et. al, 2002], but non of those peaks was observed. XRD peak of nickel oxide should occur at 37.3°, 43.4°, 62.9° and 75.3° [Gao et. al, 2008].
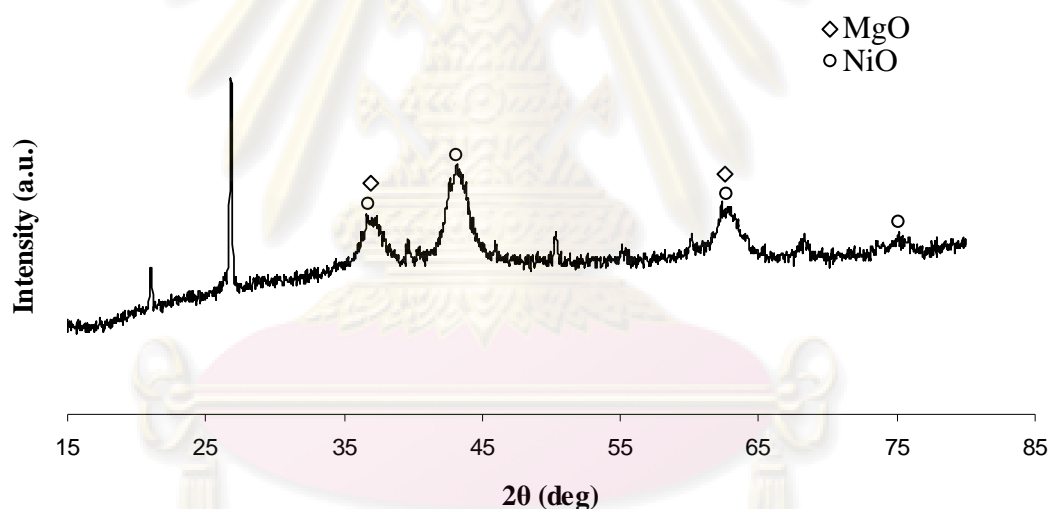

Figure 5.25 XRD patterns of the commercial Ni/SiO_2-MgO.

5.3.1.2 Nitrogen physisorption

The specific surface areas of commercial 55%wt.Ni/SiO$_2$-MgO are determined by BET technique. The results are summarized in Table 5.10.

Table 5.10 Physical properties of catalysts.

Catalysts	Specific surface area, m^2/g	Pore volume, cm^3/g	Pore size, (A°)
Ni/ C50G50-Al$_2$O$_3$	160	0.47	73.3
Ni/SiO$_2$-MgO	105	0.16	59.2

5.3.1.3 Ammonia temperature-programmed desorption (NH$_3$-TPD)

The NH$_3$-TPD profiles for commercial 55%wt.Ni/SiO$_2$-MgO are shown in Figure 5.26. The profiles are composed of two peaks, i.e. a high temperature peak representing strong acid sites and a low temperature one refering to weak acid sites. Figure 5.26 showed one shaft peak and one broad peak during the temperature range of 40 to 240°C and 240 to 500°C. The acid properties of the alumina catalysts are also reported in Table 5.11. Table.5.11 showed 55%wt.Ni/SiO$_2$-MgO has the higher acidity than that of 7%wt.Ni/50%χ-γ-alumina.
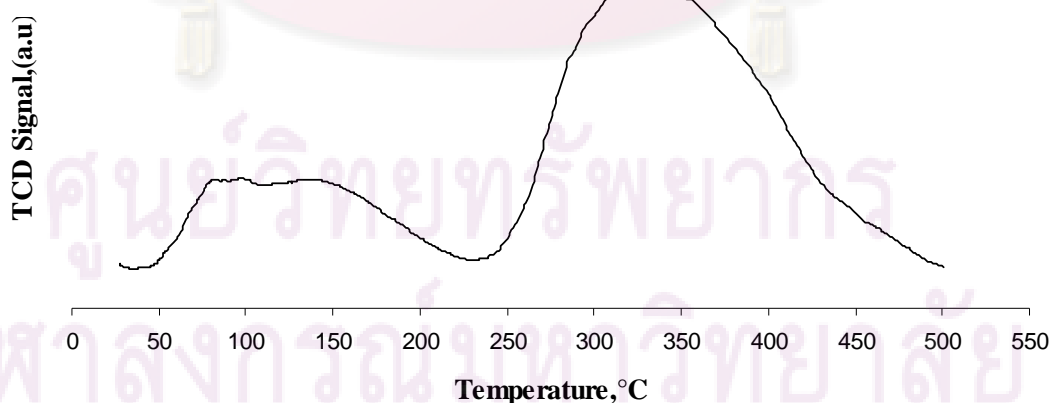

Figure 5.26 The NH$_3$-TPD profile of commercial Ni/SiO$_2$-MgO.

Table 5.11 Acidity of catalysts.

Catalysts	Adsorbed volume of ammonia, (ml)	Total acid site, (mmol H^+/g)
Ni/ C50G50-Al$_2$O$_3$	29.76	12.15
Ni/SiO$_2$-MgO	35.03	14.07

5.3.1.4 CO-chemisorption

Active site of catalysts can be determined by calculation from amount of carbon monoxide adsorption on catalysts. From Table 5.12, the 55%wt.Ni/SiO$_2$-MgO has the higher active site than that of 7%wt.Ni/50%χ-γ-alumina. The crystallite size and percent dispersion of nickel catalyst can be determined by calculated from amount of carbon monoxide adsorption on catalysts that shown in Appendix C. The 7%wt.Ni/50%χ-γ-alumina has smaller dispersed than that of the 55%wt.Ni/SiO$_2$-MgO. The crystallite size of 7%wt.Ni/50%χ-γ-alumina has bigger than that of the 55%wt.Ni/SiO$_2$-MgO. The data of crystallite size and percent dispersion of nickel catalyst is shown in Table 5.12.

Table 5.12 showed amount of carbon monoxide adsorbed on catalysts.

Catalysts	Active site, Molecule*10^{-18} per gram	% dispersion of nickel	crystallite size of Ni, nm
Ni/ C50G50-Al$_2$O$_3$	34.90	2.67	38.35
Ni/SiO$_2$-MgO	102.43	3.22	31.78

5.3.1.5 Hydrogen Temperature Programmed Reduction (H$_2$-TPR)

H$_2$-TPR pattern of nickel catalysts on support are shown in Figure.5.27. The reduction peak of free NiO species occurs at 400 ºC, which have weak interaction with support. That showed nickel catalyst on alumina is NiO species. The reduction peak of complex NiO$_x$ species will occur at above 800 ºC, which have strong

interaction with support. Based on the TPR profiles, it indicated that nickel oxide dispersed on the silica-magnesium exhibited the lower maximum reduction temperature than that of the mixed phase of alumina support.
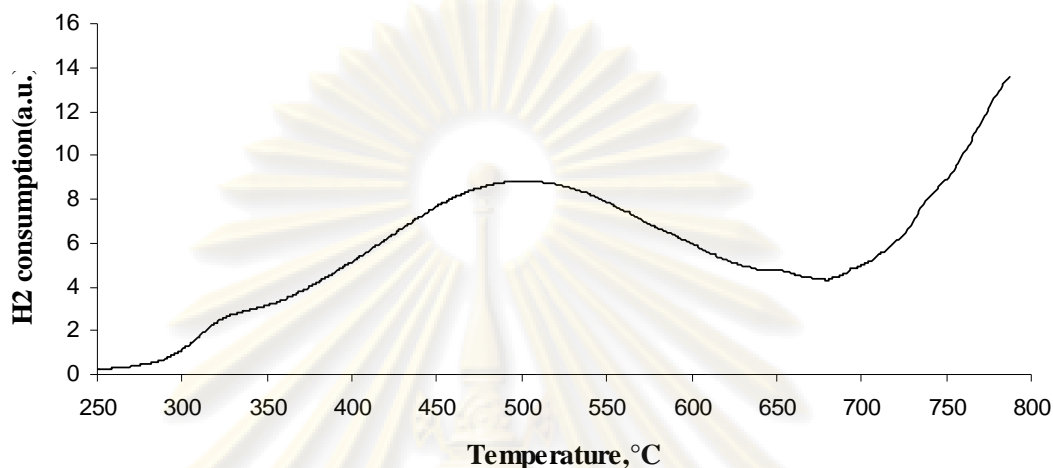

Figure 5.27 H_2-TPR pattern of commercial Ni/SiO_2-MgO.

5.3.2 Reaction study catalytic activity of nickel catalyst on mixed phase of alumina compared with nickel catalyst on silica-magnesium

Table 5.13 presents methane and carbon dioxide conversion for reforming reaction of methane by carbon dioxide over nickel catalyst. The Ni/SiO_2-MgO gave the higher methane conversion than that of Ni/C50G50 at initial time. But the Ni/SiO_2-MgO gave the smaller carbon dioxide conversion than that of Ni/ C50G50. The catalytic activity of nickel catalysts on commercial Ni/SiO_2-MgO relates directly with the active site. From table was found The Ni/ C50G50 gave the higher stability than that of Ni/SiO_2-MgO. It is due to reactor blockage in during reaction for Ni/SiO_2-MgO catalyst.

**Table 5.13** showed percent conversion of commercial Ni/SiO_2-MgO.

Time, min	Ni/C50G50[a]		Ni/SiO_2-MgO[b]	
	$\%X_{CH4}$	$\%X_{CO2}$	$\%X_{CH4}$	$\%X_{CO2}$
30	82	87	88	75
60	82	86	-	-
90	81	85	-	-
120	81	85	-	-
150	83	87	-	-
180	83	88	-	-
240	83	87	-	-
300	83	88	-	-
360	83	88	-	-

[a] 7%wt. Ni loading

[b] 55%wt. Ni loading

5.3.2.1 Morphology

The morphology characterized by Scanning Electron Microscopy (SEM). Figure.5.28 shows the SEM images of fresh catalyst and used catalysts. A lot more filament carbon species was not clearly occurred on used catalyst.
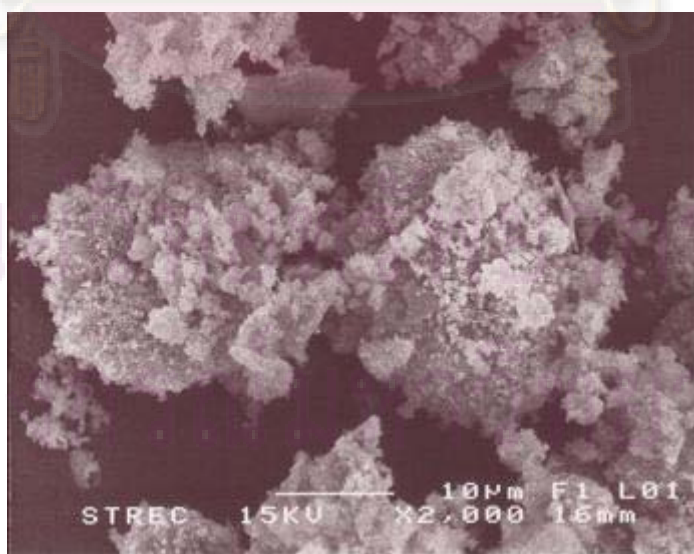
Figure 5.28 (a) The SEM images showed fresh commercial Ni/SiO_2-MgO catalyst.
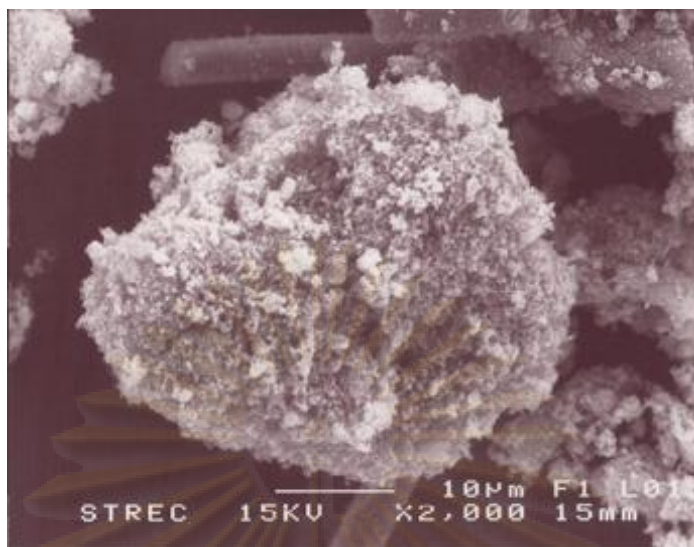
Figure 5.28 (b) The SEM images showed used commercial Ni/SiO$_2$-MgO catalyst.

5.3.2.2 Transmission Electron Microscope (TEM)

Figure.5.29 showed used catalysts characterized by TEM techniques. The filamentous carbon found was long hollow filament with possibly nickel crystallite at filament tip. This supposed to be whisker coke which does not affect the catalytic activity, but results in a pressure drop due to reactor blockage.
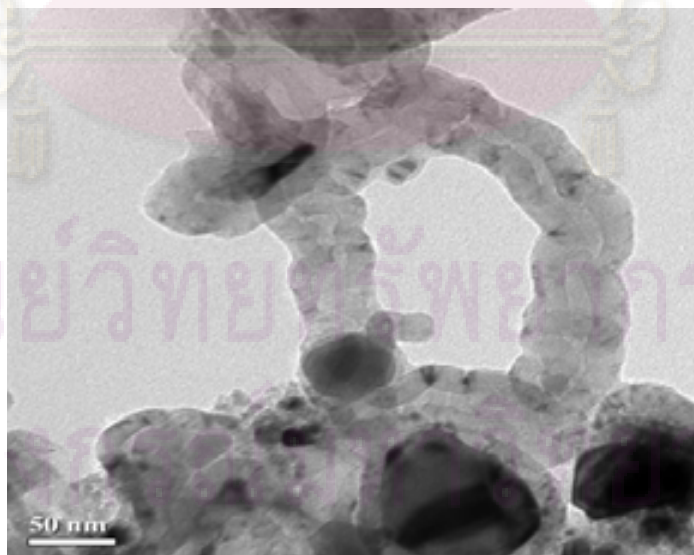

Figure 5.29 The TEM images showed filamentous carbon on used commercial Ni/SiO$_2$-MgO catalysts.

5.3.2.3 Amount of coke

Amount of coke was characterized by Thermogravimetric and differential thermal analysis (TG-DTA) which showed in Figure 5.30. It was found that the Ni/SiO_2-MgO catalysts contains weight loss the same as that of Ni/ C50G50.
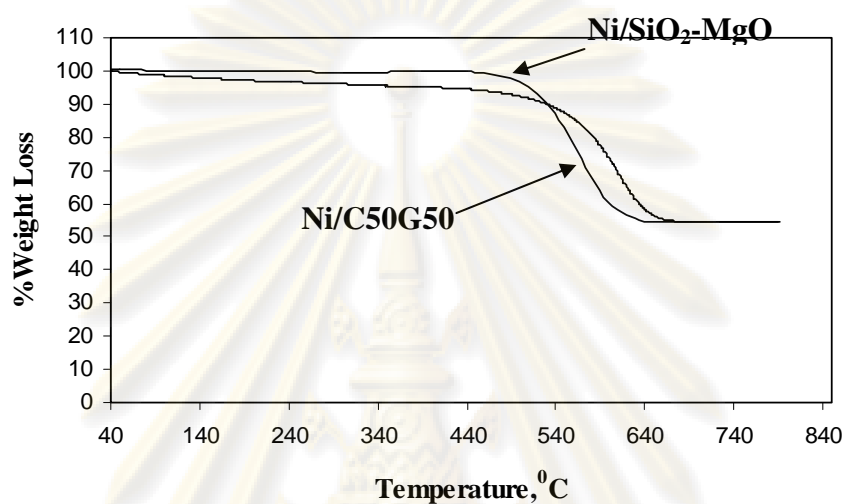

Figure 5.30 TG profiles of used catalysts under air.

CHAPTER VI

CONCLUSIONS AND RECOMMENDATIONS

6.1 Conclusions

The 7%Ni/50%χ-γ-alumina catalyst in the reforming reaction of methane by carbon dioxide exhibited the highest conversion as well as the highest coke resistance of all the catalysts studied. The mixed phase alumina has higher activity and stability than that of zeolite Y supported nickel catalysts. The commercial silica-magnesium oxide supported nickel catalyst exerted higher conversion than did the mixed phase alumina supported one; however, the mixed phase alumina supported catalyst still showed essentially better stability.

6.2 Recommendations

From this experiment, we have expected to improve acidity of catalyst for syngas production. Recommendations for the future work are the following:

1. To determine type of acidity (Bronsted and Lewis) with Fourier Transform Infrared Spectrophotometer (FTIR) for synthetic alumina.

2. To study interaction of nickel catalyst on synthetic alumina by X-Ray photoelectron spectroscopy.

3. To study effect of various χ-phase contents of alumina support, i.e. 20%χ-γ-alumina.

4. To study effect of mixed phase of synthetic titania and/or zirconia.

REFERENCES

Aramendıa, M.A., Borau, V., Jimemez, C., Marinas, J.M., Ruiz, J.R., and Urbano F.J. Influence of the preparation method on the structural and surfaceproperties of various magnesium oxides and their catalytic activity in the Meerwein–Ponndorf–Verley reaction. Applied Catalysis A: General 244, (2003): 207–215

Castro Luna, A.E., and Iriarte, M.E. Carbon dioxide reforming of methane over a metal modified Ni-Al$_2$O$_3$ catalyst. Applied Catalysis A: General 343, (2008): 10–15

Charienseri, S. Combined carbon dioxide reforming and partial oxidation of methane under periodic operation. Chulalongkorn university. Master's Thesis, Department of Chemical Engineering, Fuculty of Engineering, Chulalongkorn university, 2007.

Guo, J., Hou, Z., Gao, J., and Zheng, X. Syngas production via combined oxy-CO$_2$ reforming of methane over Gd$_2$O$_3$-modified Ni/SiO$_2$ catalyst in a fluidized-bed reactor. Fuel., (2007)

Hagen, J. Industrial Catalysis 2nd. Germany: Wiley-vch, 2006.

Halliche, D., Cherifi, O., and Auroux, A. Microcalorimetric studies and methane reforming by CO$_2$ on Ni-based zeolite catalysts. Thermochimica Acta 434, (2005): 125–131

Kaengsilalai, A., Luengnaruemitchai, A., Jitkarnka, S., and Wongkasemjit, S. Potential of Ni supported on KH zeolite catalysts for carbon dioxide reforming of methane. Journal of Power Sources 165, (2007): 347-352

Kang,J.S., Kim, D.H., Lee, S.D., Hong, S.I., and Moon, D.J. Nickel-based tri-reforming catalyst for the production of synthesis gas. Applied Catalysis A: General 332, (2007): 153-158

Khom-in, J. Synthesis of dimethylether (DME) from dehydration of methanol using γ-Al$_2$O$_3$ and γ-χ-Al$_2$O$_3$ catalysts. Master's Thesis, Department of Chemical Engineering, Fuculty of Engineering, Chulalongkorn university, 2007

Murata, S., Hatanaka, N., Inoue, H., Kidena, K., and Nomura, M. CO$_2$ reforming of methane catalyzed by Ni-Loaded zeolite-base catalysts. Greenhouse Gas Control Technologies , 2(2003): 1485-1489

Pawelec, B., Damyanova, S., Arishtirova, K., Fierro, J.L.G., and Petrov, L. Structural and surface features of PtNi c atalysts for reforming of methane with CO_2 . Applied Catalysis A: General 323, (2007): 188-201

Rui, W., Xuebin, L., Yanxin, C., Wenzhao, L., and Hengyong, X. Effect of Metal-Support Interaction on coking Resistance of Rh-based catalyst in CH_4/CO_2 reforming. Chinese Chinese Journal of Catalyst 28, (2007): 865-859

Wang, H.Y., and Ruckenstein, E. Carbon dioxide reforming of methane to synthesis gas over supported rhodium catalysts: the effect of support. Applied Catalysis A: General 204, (2000): 143-152

Wang, S., and Lu, G.Q.M. CO_2 reforming of methane on Ni catalysts: Effect of the support phase and preparation technique. Applied Catalysis B: Envirnmental 16, (1997): 269-277
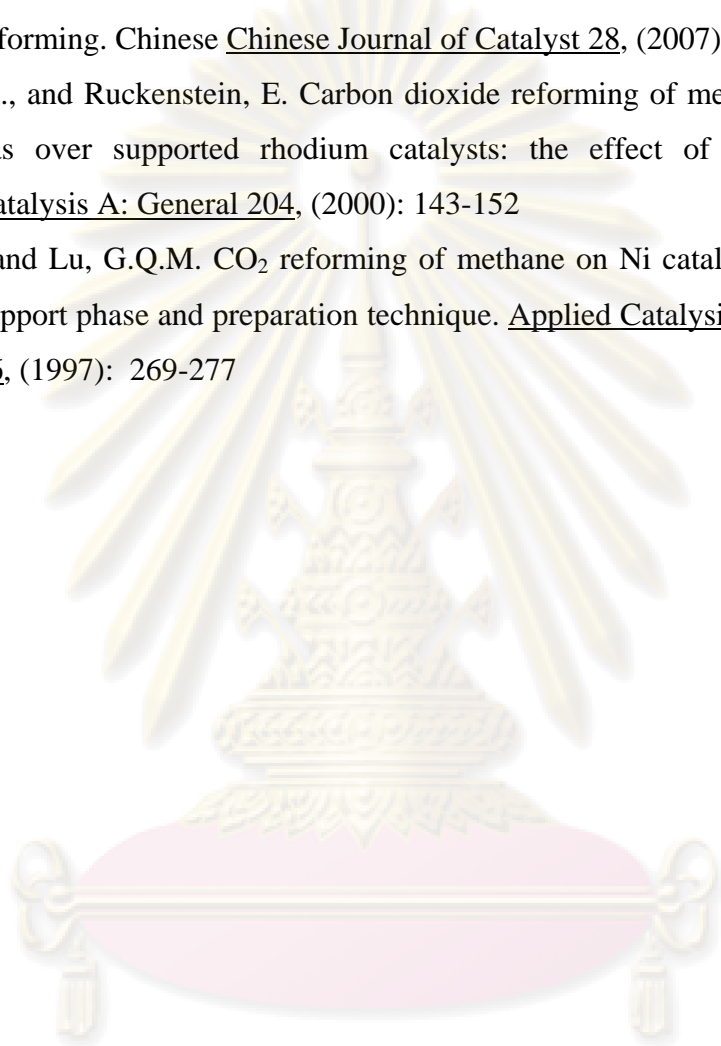
APPENDICES

ศูนย์วิทยทรัพยากร
จุฬาลงกรณ์มหาวิทยาลัย

APPENDIX A

CALCULATIONS OF REACTION FLOW RATE

Sample of calculation

The used catalyst   =   0.20 g

Pack catalyst into quartz reactor (inside diameter = 0.49 cm)

Volumetric flow rate   =   100 ml/min

Determine the average high of catalyst bed = 1.46 cm, so that

Volume of bed = $\pi(0.245)^2 \times 1.46$ = 0.275 ml

GHSV   =   Volumetric flow rate[1]/ Volume of bed

GHSV   =   100 (ml/ min)/ 0.275 ml

GHSV   =   363.64 min^{-1}

GHSV   =   363.64 $\times 60 = 21818.18$ h^{-1}

At STP condition:

Volumetric flow rate   =   Volumetric flow rate[1] $\times((273.15+T)/ (273.15))$

Where T = room temperature

APPENDIX B

CALIBRATION CURVES

This appendix shows the calibration curves for calculation of composition of products in reforming reaction of methane by carbon dioxide over supported nickel catalysts. The main product of reforming reaction of methane is carbon monoxide, carbon dioxide, hydrogen and methane.

The Thermal Conductivity Detector (TCD), gas chromatography Shimadzu model 8A was used to analyze the concentration of product by using porapack-Q column.

Mole of reagent in y-axis and area reported by gas chromatography in x-axis are exhibited in the curves. The calibration curves of carbon monoxide, carbon dioxide, hydrogen and methane are illustrated in Figure B1-B4, respectively.
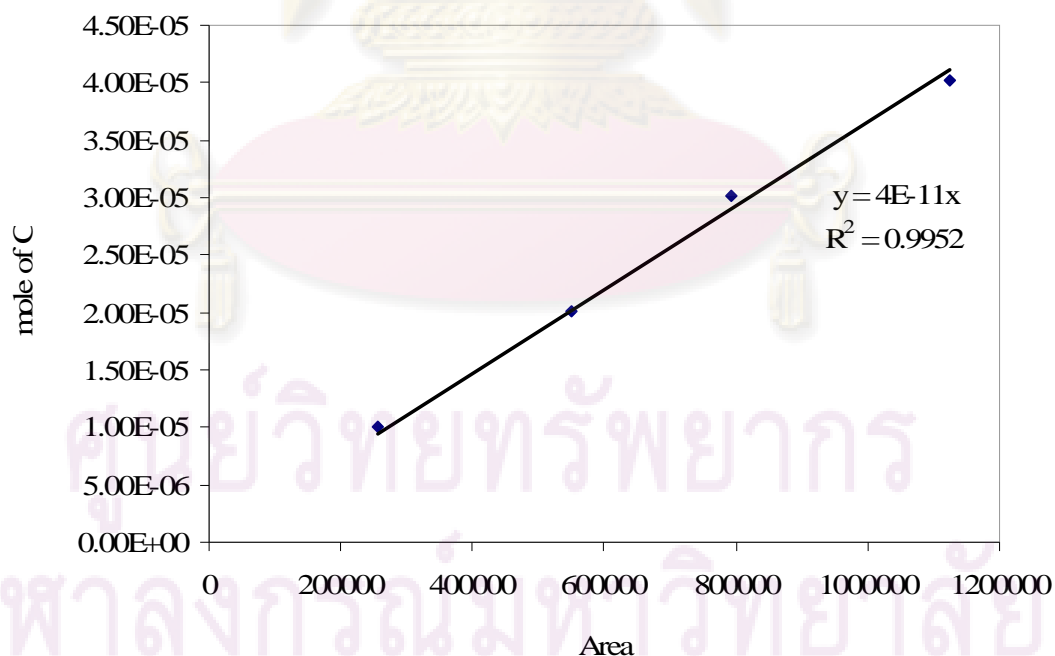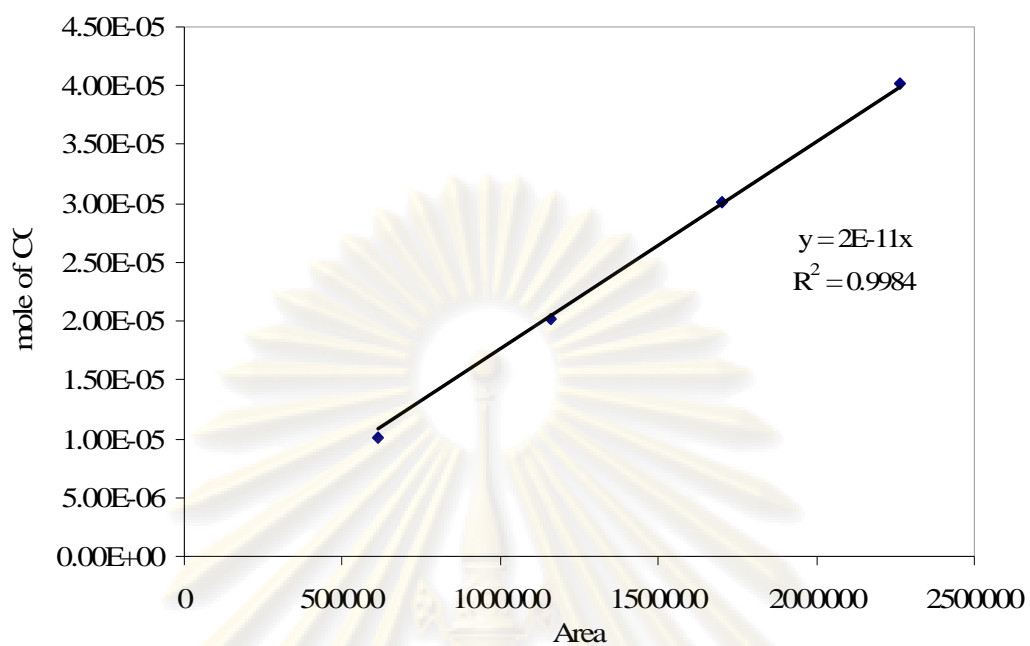

Figure B1 The calibration curve of carbon monoxide.
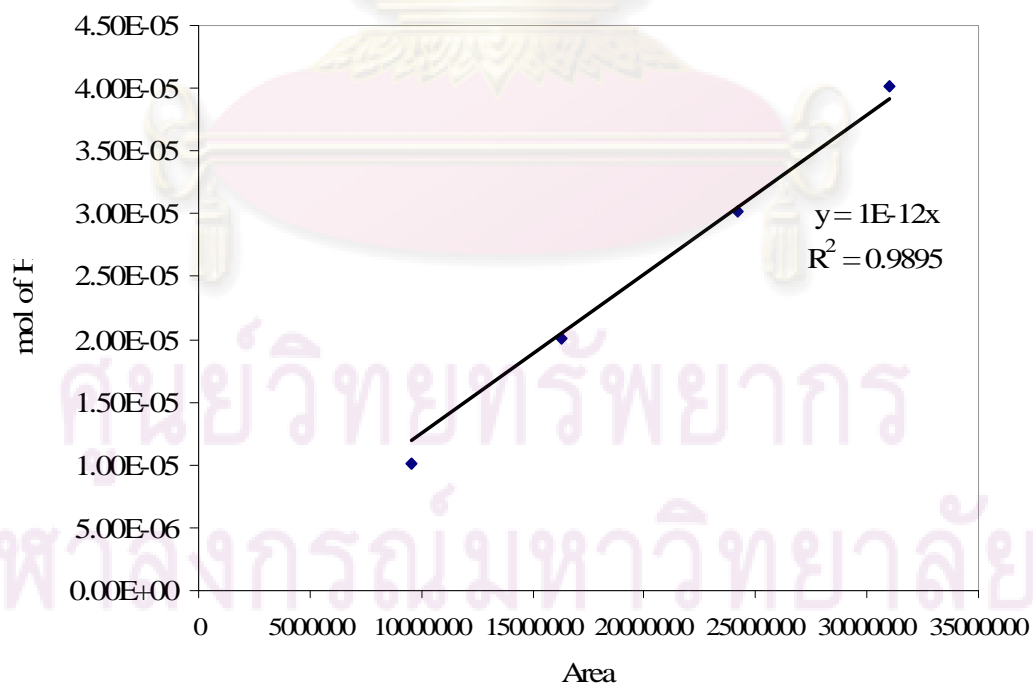
Figure B2 The calibration curve of carbon dioxide.

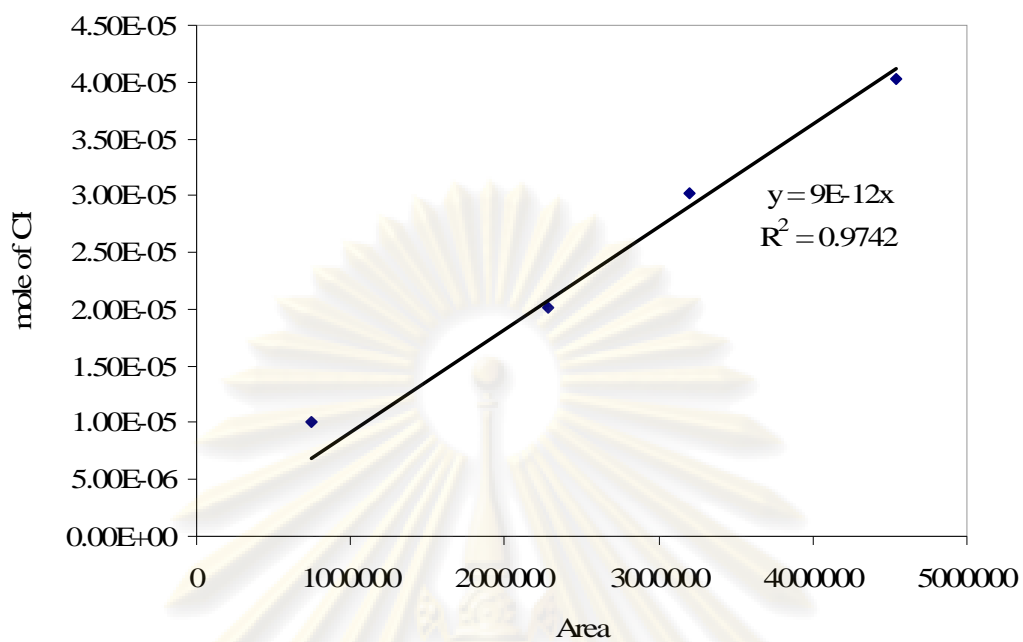**Figure B3** The calibration curve of hydrogen.

Figure B4 The calibration curve of methane.

APPENDIX C

CALCULATION FOR METAL ACTIVE SITES AND DISPERSION

Calculation of the metal active sites and metal dispersion of the catalyst measured by CO adsorption is as follows:

Calculation of metal active site

Let the weight of catalyst used	= W	g.
Integral area of CO peak after adsorption	= A	unit.
Integral area of 86 µl of standard CO peak	= B	unit.
Amounts of CO adsorbed on catalyst	= B-A	unit.
Volume of CO adsorbed on catalyst	= 86×[(B-A)/B]	µl.
Volume of 1 mole of CO at 30°C	= 24.86×10^6	µl.
Mole of CO adsorbed on catalyst	= $[(B-A)/B] \times [75/24.86 \times 10^6]$ mole.	
Molecule of CO adsorbed on catalyst	= $[3.02 \times 10^{-6}] \times [6.02 \times 10^{23}] \times [(B-A)/B]$	
	molecules.	
Metal active sites	= $1.82 \times 10^{18} \times [(B-A)/B] \times [1/W]$ molecules of	
	CO/g of catalyst.	

Calculation of %metal dispersion

Definition of % metal dispersion :

Metal dispersion (%) = 100×[molecules of Ni from CO adsorption/molecules of Ni loaded]

In this study, the formula from Chemisorb 2750 Operator's Manual can used for determined the % metal dispersion as follow:

$$\%D = S_f \text{ x } [\frac{Vads}{Vg}] \text{ x } [\frac{m.w.}{\%M}] \text{ x } 100\% \text{ x } 100\% ....(1)$$

Where

%D = %metal dispersion

S_f = stoichiometry factor, (CO on Ni* =1)

V_{ads}	=	volume adsorbed	(cm^3/g)
V_g	=	molar volume of gas at STP = 22414 (cm^3/mol)	
$m.w.$	=	molecular weight of the metal	(a.m.u.)
$\%M$	=	%metal loading	

Example: %Dispersion of 7%Ni/Al_2O_3

- Calculation Volume Chemisorbed (V_{ads})

$$V_{ads}(\mu L) = [\frac{Vinj}{m}] \times \sum_{i=1}^{n}(1-\frac{Ai}{Af}) \dots\dots\dots\dots\dots(2)$$

Where:

V_{ing}	=	volumn injected (cm^3) = 77.48 μL
m	=	mass of sample (g)
Ai	=	area of peak i
Af	=	area of last peak

To replace values in equation (1) and (2);

$$V_{ads} = [\frac{77.48}{0.2008}] \times [(1-\frac{0.00047}{0.008187})+(1-\frac{0.00209}{0.008187})+(1-\frac{0.00686}{0.008187})]$$

$$= 713.59 \ \mu L$$

$$\%D = 1 \times [\frac{77.48}{22414*10^3}] \times [\frac{58.710}{7}] \times 100\% \times 100\%$$

$$= 2.67\%$$

So that %Ni dispersion is 2.67%

Calculation of average crystallite size

The formula from Chemisorb 2750 Operator's Manual can used for determined the % metal dispersion as follow:

$$d = [\frac{F_g}{\rho \times MSA_m}] \times [\frac{m^3}{10^6 \ cm^3}] \times \frac{10^9 \ nm}{m} \dots\dots\dots\dots(1)$$

Where

d	=	Average crystallite size
F_g	=	Crystallite geometry factor (hemisphere =6,
		Cube =5)
ρ	=	Specific gravity of the active metal, (g /cm^3)
MSA_m =		Active metal surface area per gram of metal, (m^2/g metal)

Example: Average crystallite size

- Calculation active metal surface area per gram of metal (MSA$_m$)

$$MSA_m(m^2/gmmetal) = S_f \times [\frac{V_{ads}}{V_g}] \times [\frac{100\%}{\%M}] \times [N_A] \times [\sigma_m] \times [\frac{m^2}{10^{18}nm^2}]...............(2)$$

Where:

S_f	=	stoichiometry factor, (CO on Ni* =1)
V_{ads}	=	volume adsorbed, (cm^3/g)
V_g	=	molar volume of gas at STP = 22414 cm^3/mol
$\%M$	=	weight percent of the active metal
N_A	=	Avogadro's number = 6.023 x 10^{23} molecules/ mol
σ_m	=	cross-sectional area of avtive metal atom, nm^2

So, that

$$MSA_m(m^2/gmmetal) = 1 \times [\frac{713.59\,\mu L}{22.414 \times 10^6\,\mu L}] \times [\frac{100\%}{7\%}] \times [6.023 \times 10^{23}] \times [0.0649]$$

$$\times [\frac{m^2}{10^{18}nm^2}] = 17.78 \text{ m}^2/\text{g metal}$$
...............................(2)

To replace values in equation (1) and (2);

$$d = [\frac{6}{8.8 \times 26.84}] \times [\frac{m^3}{10^6\,cm^3}] \times \frac{10^9\,nm}{m} ....(1)$$

d = 38.35 nm

So that average crystallite size is 38.35 nm

APPENDIX D

DATA OF CALCULATION OF ACID SITE

Calulation of total acid sites

For example, TS-1 sample, total acid site is calculated from the following step.

  1. Conversion of total peak area to peak volume

conversion from Micromeritrics Chemisorb 2750 is equal to 77.5016 ml/area unit. Therefore, total peak volume is derived from

Example: Ni/C50C50 catalyst give total peak area is 2.55975 area

$$
\begin{aligned}
\text{Total peak volume} \quad &= 77.5016 \times \text{total peak area} \\
&= 77.5016 \times 2.55975 \\
&= 198.39 \text{ ml}
\end{aligned}
$$

  2. Calculation for adsorbed volume of 15% NH_3

$$
\begin{aligned}
\text{adsorbed volume of 15\% } NH_3 \quad &= 0.15 \times \text{total peak volume} \\
&= 0.15 \times 198.39 \text{ ml} \\
&= 29.76 \text{ ml}
\end{aligned}
$$

  3. Total acid sties are calculated from the following equation

$$
\text{Total acid sites} = \frac{(\text{Adsorbed volume, ml}) \times 101.325\,\text{Pa}}{\left(8.314 \times 10^{-3}\,\dfrac{\text{Pa} \cdot \text{ml}}{\text{K} \cdot \mu\text{mol}}\right) \times 298\,\text{K} \times (\text{weight of catalyst, g})}
$$

For Ni/C50C50 catalyst sample , 0.1001 g of this sample was measured, therefore

$$\text{Total acid sites} = \frac{29.76\,\text{ml} \times 101.325\,\text{Pa}}{\left(8.314 \times 10^{-3}\,\dfrac{\text{Pa} \cdot \text{ml}}{\text{K} \cdot \mu\text{mol}}\right) \times 298\,\text{K} \times (0.1001\,\text{g})}$$

$$= 12.158\ \text{mmol H}^+/\text{g}.$$

APPENDIX E

CALIBRATION CURVE OF CHI PHASE PERCENT

This appendix showed the calibration curves for calculation of chi phase percent in alumina catalysts which derived from the XRD pattern of physical mixtures between pure γ- and χ- alumina with various contents.[Khom-in, 2007]
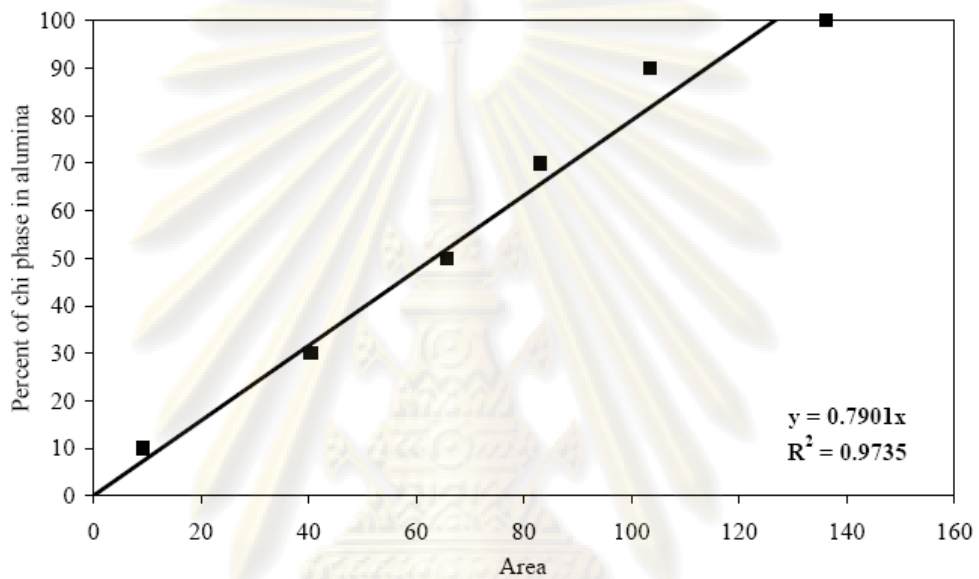

Figure E1 The calibration curve of chi phase percent in alumina.
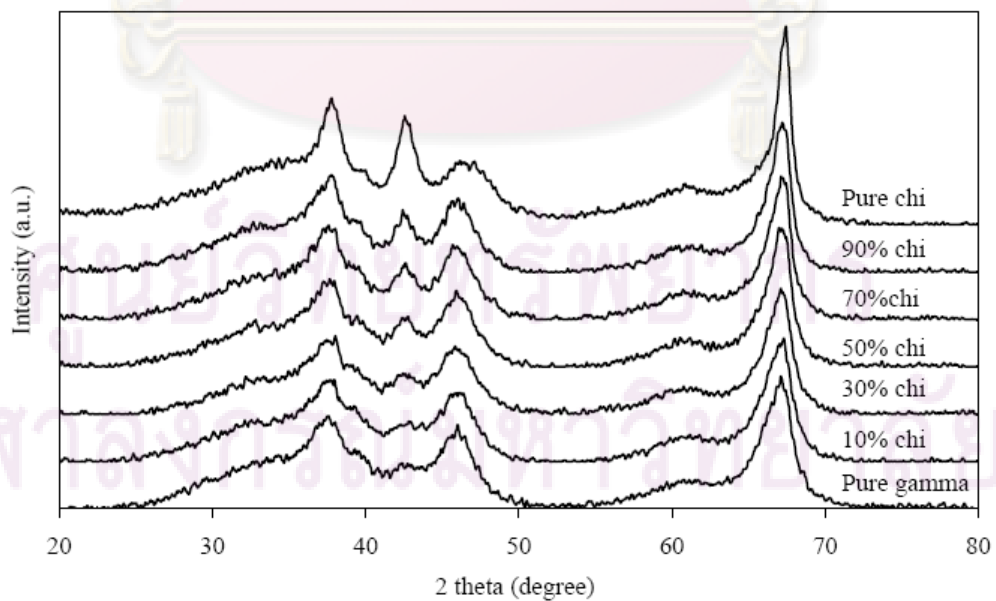

Figure E2 The XRD pattern of physical mixtures between pure γ- and χ- alumina with various contents

APPENDIX F

LIST OF PUBLICATION

Nuchchanok Yoonpan, Suphot Phatanasri and Piyasan praserthdam "Reforming reaction of methane by carbon dioxide over alumina-supported nickel catalysts: The effect of alumina phase", 2nd SUT Graduate Conference., Suranaree University of Technology, Nakhon Ratchasima, Thailand, Jan., 21-22, 2009.

VITA

Miss Nuchchanok Yoonpan was born on December 14th, 1984 in Chacherngsao province, Thailand. She finished high school from Trium Udomsuksa Pattanakarn Suwintawong School in 2003, and received the bachelor's degree of Chemical Engineering from Faculty of Engineer, Burapha University in 2007. She continued her master's study at Department of Chemical Engineering, Faculty of Engineering, Chulalongkorn University in June, 2007.